SERDP

FINAL REPORT

Wave Resolved and Averaged Numerical Modelling of UXO Migration

Peter Traykovski
Woods Hole Oceanographic Institution

Margaret Palmsten
United States Geological Survey

September 2023

SERDP Project MR21-1341

REPORT DOCUMENTATION PAGE

Form Approved
OMB No. 0704-0188

1. REPORT DATE *(DD-MM-YYYY)*	**2. REPORT TYPE**	**3. DATES COVERED** *(From - To)*
21/06/2023	SERDP Final Report	5/14/2021 - 5/14/2023

4. TITLE AND SUBTITLE

Wave Resolved and Averaged Numerical Modelling of UXO Migration

5a. CONTRACT NUMBER
21-C-0035

5b. GRANT NUMBER

5c. PROGRAM ELEMENT NUMBER

6. AUTHOR(S)
Peter Traykovski
Woods Hole Oceanographic Institution

Margaret Palmsten
United States Geological Survey

5d. PROJECT NUMBER
MR21-1341

5e. TASK NUMBER

5f. WORK UNIT NUMBER

7. PERFORMING ORGANIZATION NAME(S) AND ADDRESS(ES)
Woods Hole Oceanographic Institution
Applied Ocean Physics and Engineering
266 Woods Hole Road, Bigelow 109A (MS #12)
Woods Hole, MA 02543-1535

8. PERFORMING ORGANIZATION REPORT NUMBER
MR21-1341

9. SPONSORING/MONITORING AGENCY NAME(S) AND ADDRESS(ES)
Office of the Deputy Assistant Secretary of Defense (Energy Resilience & Optimization)
3500 Defense Pentagon, RM 5C646
Washington, DC 20301-3500

10. SPONSOR/MONITOR'S ACRONYM(S)
SERDP

11. SPONSOR/MONITOR'S REPORT NUMBER(S)
MR21-1341

12. DISTRIBUTION/AVAILABILITY STATEMENT

DISTRIBUTION STATEMENT A. Approved for public release: distribution unlimited.

13. SUPPLEMENTARY NOTES

14. ABSTRACT

One of the critical areas for underwater munition detection and remediation is very shallow water less than 5 m deep. The very shallow water emphasis comes from the fact that munitions are most likely to be encountered by the general public in depths that are suitable for wading, swimming, and scuba diving, with potential encounters more likely in the shallowest water. In many environments there will be occasional to frequent breaking waves in depths from 0.5 m to 3 m. In this region Unexploded Ordnances (UXO) may either bury, remain proud of the seafloor, or become re-exposed. In environments with energetic forcing or steep slopes the UXO may migrate. Numerical modelling of environmental conditions and UXO response is a powerful tool
to assess the relative likelihood of these processes. The overall objective of the work was to improve models for hydrodynamic forcing of UXO migration and burial in shallow water surfzone environments. Our work addressed the following questions:
-Does the balance between onshore forcing by wave asymmetry and skewness and offshore forcing by return flows control mobile UXO location in the surf-zone?
-Are the wave asymmetry, skewness and return flow processes in the surf zone represented by phase averaged models adequately to reproduce observed UXO migration events?
-What is the role of morphology (e.g., migration of sandbars) in UXO burial and migration and can this be captured by phase resolving models?

15. SUBJECT TERMS

Wave Resolved Numerical Modelling, Averaged Numerical Modelling, UXO Migration, UXO, UXO Mobility, water column

16. SECURITY CLASSIFICATION OF:			**17. LIMITATION OF ABSTRACT**	**18. NUMBER OF PAGES**	**19a. NAME OF RESPONSIBLE PERSON**
a. REPORT	**b. ABSTRACT**	**c. THIS PAGE**			Peter Traykovski
UNCLASS	UNCLASS	UNCLASS	UNCLASS	42	**19b. TELEPHONE NUMBER** *(Include area code)* 508-289-2638

Executive Summary

1. Introduction

One of the critical areas for underwater munition detection and remediation is very shallow water less than 5 m deep. The very shallow water emphasis comes from the fact that munitions are most likely to be encountered by the general public in depths that are suitable for wading, swimming, and scuba diving, with potential encounters more likely in the shallowest water. In many environments there will be occasional to frequent breaking waves in depths from 0.5 m to 3 m. In this region Unexploded Ordnances (UXO) may either bury, remain proud of the seafloor, or become re-exposed. In environments with energetic forcing or steep slopes the UXO may migrate. Numerical modelling of environmental conditions and UXO response is a powerful tool to assess the relative likelihood of these processes. The overall objective of the work was to improve models for hydrodynamic forcing of UXO migration and burial in shallow water surf-zone environments. Our work addressed the following questions:

- Does the balance between onshore forcing by wave asymmetry and skewness and offshore forcing by return flows control mobile UXO location in the surf-zone?
- Are the wave asymmetry, skewness and return flow processes in the surf zone represented by phase averaged models adequately to reproduce observed UXO migration events?
- What is the role of morphology (e.g., migration of sandbars) in UXO burial and migration and can this be captured by phase resolving models?

The research used both a wave-resolving model (SWASH) that explicitly computes non-linear wave transformations and a wave-averaged model (XBeach) that parametrizes nonlinear transformations in terms of wave asymmetry and skewness. The output of these nearshore hydrodynamic models is input into a parameterized UXO burial and mobility post-processing module based on a previously developed time-dependent burial model. Our approach investigated the balance between onshore forcing by wave asymmetry and skewness and offshore forcing by return flows as described by an interpolation function calculated from the parameterized equations of motion for a cylinder. The advantage of the wave-averaged models is three-fold. First, wave-averaged models have a much lower computational expense allowing rapid modelling of larger operational areas. Second, Due to the lower computation expense longer runs which capture coastal morphodynamic change are possible. Third, wave-averaged models can span a wider parameter space and are useful for developing ensemble results for inclusion in statistical models of munitions behavior.

2. Objectives

The objectives of the work were to develop and evaluate a suite of modeling approaches to describe UXO migration trajectories in the surf zone. These models combined with observations from previous studies will be used to **assess a conceptual hypothesis that the balance between onshore forcing by wave skewness and asymmetry and offshore return flows controls the location of mobile UXO in the surf zone**. A wide range of models are available for surf zone hydrodynamics ranging from wave-averaged models such as DELFT3D coupled with SWAN, to short wave-averaged and long wave (infragravity) resolving models such as XBeach, to wave resolved models such as SWASH. In order to predict on and offshore sand bar migration, the wave-averaged models have parametrized descriptions of wave skewness (*Sk*) and asymmetry (*As*), while the wave resolving models explicitly calculate the non-linear wave transformations that control *Sk* and *As*. All of these models resolve the offshore return flows, but have significant differences, due to vertical resolution and wave driven flow formulations. **Thus, a second objective of the proposed work was to determine if the parametrized calculations of *Sk* and *As* in the wave-averaged models are sufficient to**

predict on and offshore migration, and the final deposition zones of UXO in the surf zone. The second objective will be addressed by evaluating the results of the wave-averaged models relative to wave resolving modes and observations.

The third objective was to evaluate the potential of using wave-averaged models with a wide range of input parameters to develop databases for statistical models. The motivation for a one-year MRSEED proposal as opposed to a larger effort was that it was not known a-priori without conducting the research whether the wave-averaged models will be accurate enough to achieve this third objective. One of the important results of the research is that the parametrized calculations of *Sk* and *As* in the wave-averaged models were sufficiently accurate to hindcast field observations of UXO mobility forced by non-linear wave processes.

3. Technical approach

3.1. Background

Recent field measurements (MR2319 [1], MR2729 [2], and MR2320 [3]) of the mobility, burial and re-exposure of munitions have significantly increased our knowledge of the parameters that control mobility and burial. The measurements in MR2319 conducted on the South Shore of Martha's Vineyard, MA indicate that medium sized (D = 7 and 15 cm, L = 75 cm) low density surrogate UXO ($\rho_0 < 2.5$ g/cm^3) were observed to migrate up to 160 m onshore, across the surf zone (Figure ES-1), while denser objects buried in place in response to waves with 2.5 m significant wave height (H_s).

In contrast, in a more recent field deployment conducted in winter of 2018 (MR2729) at the same location with similar surrogate UXO, but much larger waves (H_s = 3.5 m), little to no large-scale onshore migration was measured despite the more energetic forcing and evidence of small-scale object mobility (Figure ES-2). In the more recent deployment, while the surrogate UXO did not migrate the sand bar migrated from a location near the beach to the location where the UXO were deployed in 3 to 4 m water depth, burying the UXO in up to 1.5 m of sand.

To help understand the physical mechanisms that led to onshore migration in moderate height waves and no migration with larger waves as part of MR2729, the output from a wave resolving numerical model for surf-zone hydrodynamics (SWASH) was coupled with a post-processing module that includes the equation of motion for a cylindrical UXO (*Object mobility* described below) and parametrization of the time dependent burial by wave induced scour (*Object Burial* described below).

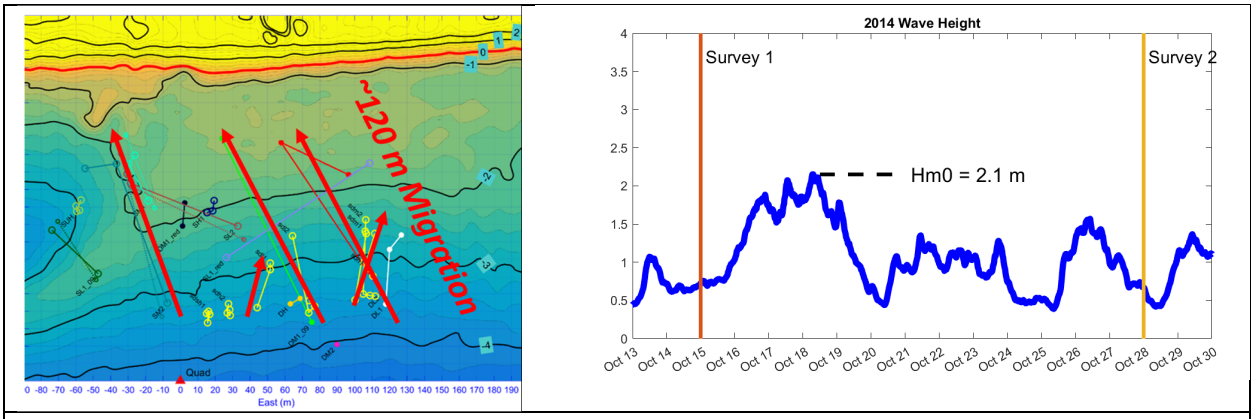

Figure ES-1. Left Panel) Bathymetry and UXO migration path from MR2319 in 2014 on the south coast of Martha's Vineyard. Right Panel) Wave Height time series

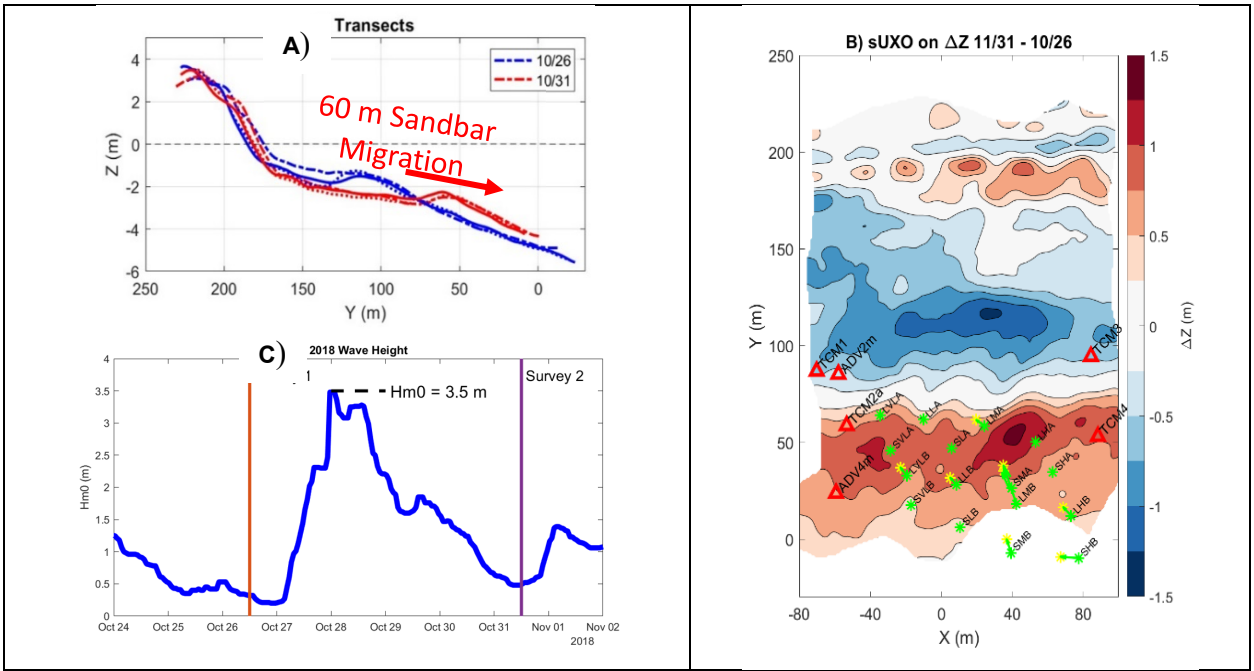

Figure ES-2. A) Bathymetry transects from MR-2729 in 2018 on the south coast of Martha's Vineyard. B) Bathymetric change map and sUXO migration paths. C) Wave Height time series

Object Mobility: The parameter space where burial versus migration is expected can be examined by considering the moments on an object resting on a deformable sand bed. In a highly simplified analysis, the moment per unit length that will induce roll of the cylinder is $T_f = FD_o(1/2 - p_b)$,where D_o is the diameter of the object, p_b is the fractional burial and is related to the depth of burial (b_d) by $p_b = b_d/D_o$. The total lateral force (F) on the object consists of the sum of three terms, the drag force (F_D), the inertial force (F_I) and the pressure gradient force (F_P), $F = F_D + F_I + F_P$. The drag force due to water motion (U) is $F_D = \rho_w C_d U|U|D_o/2$, the inertial term is $F_I = C_m \rho_w \pi D_o^2 \dot{U}/4$, and the pressure gradient term is $F_P = \rho_w \pi D_o^2 \dot{U}/4$

$C_d$and C_m are the drag and inertial coefficients. ρ_w is the water density. $\dot{U}$ is the flow acceleration. The stabilizing moment caused by the weight of the cylinder per unit length when the object is less than halfway buried is $T_w = WD_0\sqrt{p_b(1/2 - p_b)}$, based on a submerged weight of $W = \cos(\beta)(\rho_0 - \rho_w)g\pi D_0^2/4$, where $\rho_0$is the object density and β is the seafloor slope. The ratio of the destabilizing forces due to drag only and the stabilizing forces is quantified by the object Shields parameter (θ_{op_b}) based on percent burial ($p_b = b_d/D_o$) on a flat seafloor are:

$$\theta_{op_b} = \frac{C_d U|U|^2}{g(S_o - 1)D_o} \frac{2(1/2 - p_b)}{\pi\sqrt{p_b(1/2 - p_b)}} = \theta_o \frac{2(1/2 - p_b)}{\pi\sqrt{p_b(1/2 - p_b)}} \quad (1)$$

The key parameters in this expression are the diameter of the object and the initial depth of burial as these determine the moment arms, and the current velocity (U) combined with the relative density of the object (S_o) as these determine the forces.

These calculations assume a stationary object and thus are used to calculate thresholds of initial motion. For a dynamic analysis to calculate migration rate and distance the water velocity can be replaced by the relative velocity between the water and the object (U-U_0). The lateral

acceleration of the object can be calculated from a lateral force balance

$$\rho_0 \pi D_o^2 \dot{U}_o / 4 = F - \mu W + F_g, \quad (2)$$

where the friction coefficient is given by $\mu = \sqrt{p_b(1/2 - p_b)}/(1/2 - p_b)$. The downslope gravitational term (F_g) is given by $F_g = \sin(\beta)(\rho_o - \rho_w) g\, \pi D_o^2/4$. These dynamic calculations require the full phase resolved series of water velocity as the shape of the wave is important for correctly calculating the flow acceleration ($\dot{U}$). The migration distance (X) of the object can be found by double integrating the object acceleration ($\dot{U}_o$) from Eqn 2.

$$X = \iint \dot{U}_0 dt \quad (3)$$

Object Burial: Laboratory data and some field data have also been used to develop parameterized expressions for the state of burial of cylinders, mines, and ordnance-shaped objects. There is a large body of literature on this subject and the results are well summarized in Rennie, Friedrichs, and Brandt [4], [5] (henceforth referred to as RBF16). This work suggests the following expression for equilibrium burial depth:

$$p_{b,eq} = a_2 \theta_{sed}^{b_2} a_2 \Theta_{sed}^{b_2} a_{KC} KC^{b_{KC}} \quad (4)$$

The values proposed by Y. A. Cataño-Lopera and M. H. García [6] of $a_2 = 1.6$ and $b_2 = 0.85$ for wave periods of T > 4 s were used for predictions of burial depth in this study. The parameter a_{KC} was set 0.1 and b_{KC} was set to 0.51. The sediment Shields parameter is calculated from $\theta_{sed} = f_w U_{br}^2 / g(S_o - 1) d_{50}$ where the wave friction factor (f_w) is based on the expression from Nielsen [7]:

$$f_w = \exp\left(5.5\left(\frac{12 U_{br} T_p}{2\pi d_{50}}\right)^{-0.2} - 6.3\right) \quad (5)$$

where U_{br} is the near bed wave orbital velocity and T_p is the peak wave period.

The equilibrium burial depth formulations relate the final depth of burial to constant wave forcing conditions. The burial process is known to take a finite amount of time, which is related to the sediment transport rate and the size of the scour pit that the object will self-bury in. Whitehouse et al. [8] modeled time-dependent burial as a logistic process, whereby the burial depth (p_b) follows the equilibrium burial depth ($p_{b,eq}$) with a timescale (T^*):

$$\frac{dp_b}{dt} = \frac{p_{b,eq} - p_b}{T^*} \quad (6)$$

This expression is similar to that used by Traykovski et al. [9] for modeling time-dependent evolution ripple geometry. For a step change in forcing, this results in the following: $p_b(t) = p_{b,eq}(1 - \exp(-t/T^*))$. The timescale is the ratio of the object diameter squared to the sediment transport rate:

$$T^* = \frac{\alpha \theta_{sed}^N D_o^2}{(g(S_{sed} - 1) d_{50}^3)^{0.5}} \quad (7)$$

The parameter N is set to 1.5 based on the Meyer-Peter and Müller [10] sediment transport rate formulation, and the parameter α is used to tune the model to field data sets. The mobility thresholds calculated by the RBF16 method and equations 1 and 2 were compared to measurements of surrogate UXO mobility as described in the MR2719 final report. When these methods were used to calculate thresholds based on a time invariant initial burial depth of 10% the model failed to segregate the data into mobile and non-mobile classes (Figure ES-3, left).

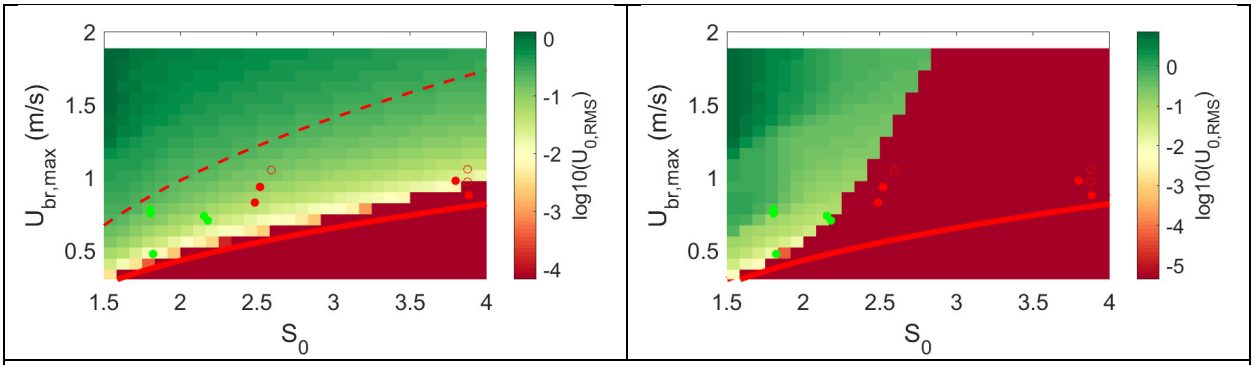

Figure ES-3. Results of the UXO migration model developed in MR2729 for (left) a constant 5% (solid red line) and 30% (dashed red line) burial depth case and (b) time dependent scour case. The red lines are thresholds predicted from methods described in RBF16 and the red and green dots are measurements of UXO migration from MR2719, in which the green dots indicate object that migrated, and the red dots indicate stationary objects.

The model was run with 5% and 30% initial burial. The model predictions are shown as a color plot of UXO root-mean-squared velocity ($U_{0,RMS}$) versus UXO relative density (S_0) and wave forcing velocity (U_w). The transition from red (stationary) to green (mobile) in the color plot compares well to the red line predicted by the RBF16 method. The methods described in the MR2319 final report and in RBF16 only predict the thresholds of mobility and are not able to predict migration rates. The method developed in MR2729 and described here predicts both the threshold and migration rates, and the threshold predictions are consistent with the previous methods.

Points above the curve are predicted to be mobile (green zone for p_b = 5%), and points below (red zone for p_b = 5%) are predicted to be stationary. The observations are plotted as green points in (U_{br}, S_o) space for mobile objects and red points for stationary objects. Both predictions for p_b of 5% (red line) and 30% (dashed red line) are inconsistent with the observations of UXO mobility. A mobility threshold curve based on an initial state of burial of 5 % incorrectly predicts that all objects, including those with S_o greater than 2.5, would be mobile. A threshold curve based on an initial state of burial of 30% incorrectly predicts that all objects, including those with S_o less than 2.5, would be stationary. Curves between 5% and 30% do not result in better predictions because the theory does not account for the dramatic change in mobility/burial behavior near a relative density of 2.2 to 2.6, which is slightly above the typical density of 2.0 for water-saturated sand beds.

3.2. Wave-Resolved Methods

The new methods developed in MR21-1341 begin with refinements to the wave resolved mobility and burial model. The first step was to break the burial and mobility into separate functions so the same function can be used in a variety of applications. Equations (1) through (9) were incorporated in the CylForceBalance.m function which updates the UXO velocity for the next time step ($U_{0,t+1}$) based on inputs of (g, β, p_b, C_d, ρ_w, ρ_o, D_o, U, $\dot{U}$, $U_{o,t}$, Δt).

The time dependent burial formulation was incorporated into a second function, BurialUpdate.m which outputs the updated time dependent burial depth and equilibrium burial depth ($p_{b,t+1}, p_{b,eq}$) based in the inputs of (g, ρ_w, ρ_o, D_o, U_{br}, T_p, d_{50}, α, $p_{b,t}$, $p_{b,min}$, $U_{o,t}$, Δt). A minimum burial of $p_{b,min} = 0.05$ is assigned so the UXO always has some deformable bed rolling friction and this was typically used as the initial condition also. A schematic of the overall computational flow chart is shown in Figure ES-4.

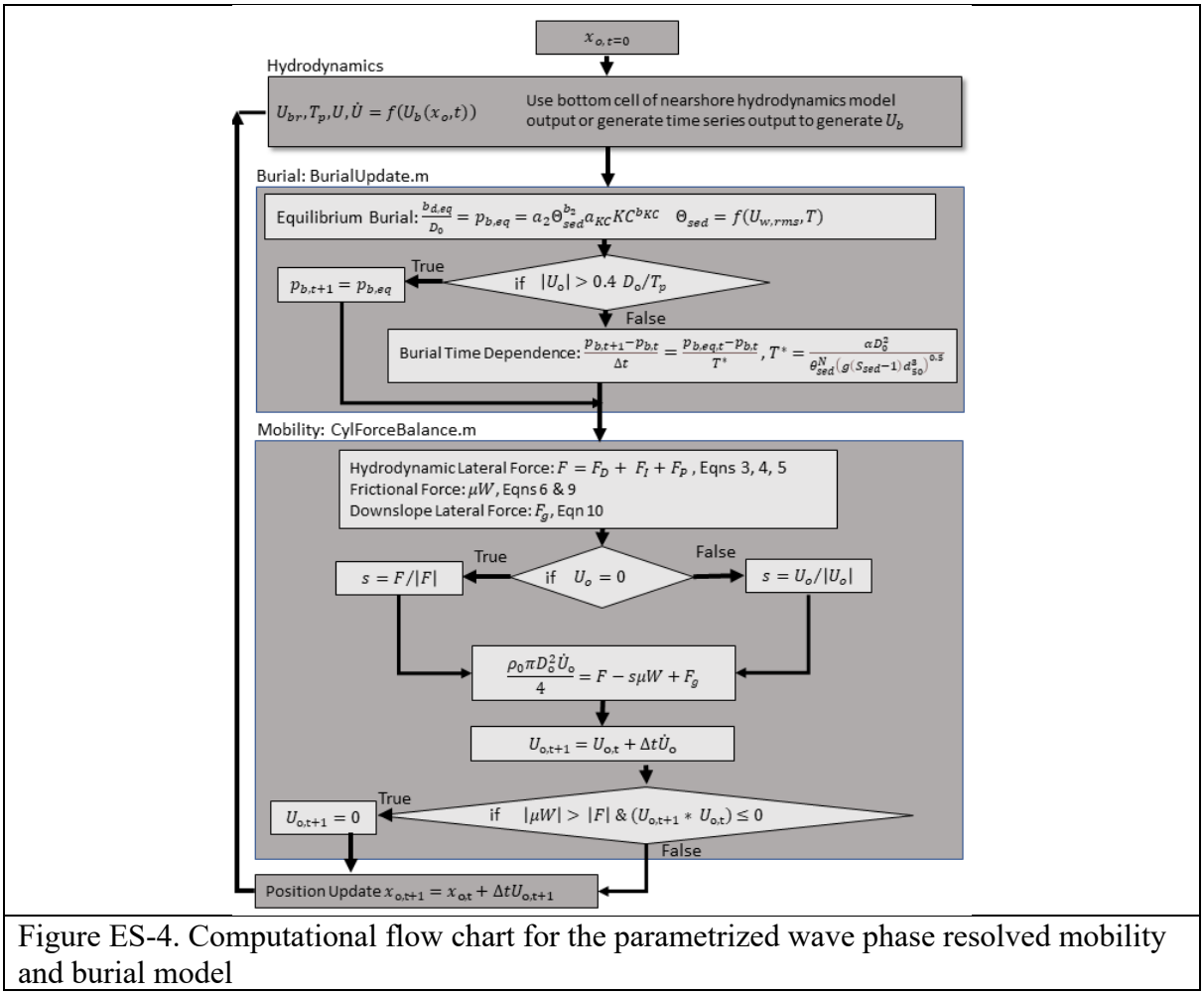

Figure ES-4. Computational flow chart for the parametrized wave phase resolved mobility and burial model

The phase resolved burial and mobility model described in the schematic can be forced with the bottom bin of the water velocity output ($U_{br},\ T_p,\ U, \dot{U} = f(U_b(x_o,t))$) from a phase resolving nearshore hydrodynamics model such as SWASH, or spatially uniform input water velocity data can be generated to span a wide range of input parameters.

3.3. Wave-Averaged Methods

In order to use the burial and mobility model with output from phase averaged models that only output variables such as $U_{br},\ T_p$ and U_c (the mean current velocity) and do not resolve the phase resolved quantities $U, \dot{U}$ the phase resolved model was run over a wide range of spatially uniform input parameters to develop a function that can be used to calculate the UXO velocity as a function of these parameters:

$$U_o = f_M(\rho_o, b_d, U_{br}, T_p, U_c, Sk, As, \beta) \tag{8}$$

A Matlab script was developed to loop over 7 to 17 steps for each parameter and run for all possible combinations of parameters and output results into an 8-dimensional matrix. The UXO diameter (D) was set at 0.15 m and the length (L) was set at 0.75 cm, but these parameters could easily be changed. UXO density (ρ_o), burial depth (b_d), representative wave orbital velocity (U_{br}) and seabed slope (β) were simply assigned values in the loop iterations. It is assumed that the burial depth does not vary over the short time scale of the input time series used to generate to the interpolation function but could change over the time step of the phase averaged

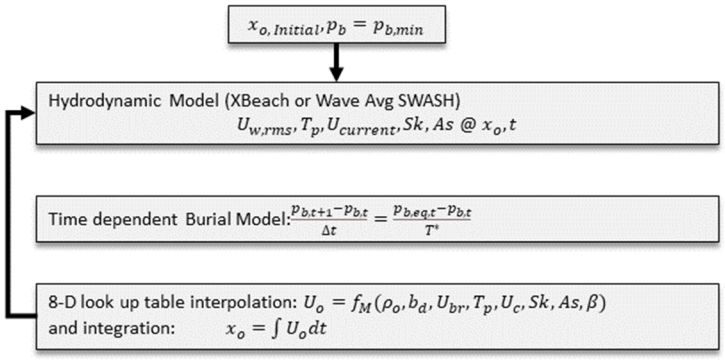

Figure ES-5. Computational flow chart for the parametrized wave phase averaged mobility and burial model.

hydrodynamics model. Combined wave (U_w) and current (U_c) velocity time series were calculated by $U = U_c + U_w$. The skewness *Sk* (0 to 1.6) and asymmetry *As* (-1.6 to 0) range are selected based on values found in field environments and predicted by the nearshore hydrodynamics models.

The computational workflow for the wave-averaged model is similar to phase resolved model except instead of using the full equations of motion for UXO migration velocity the interpolation function is used and the input is from a wave-averaged nearshore hydrodynamics model such as XBeach. A simplified schematic of the workflow is shown in Figure ES-5. For testing purposes, the wave-averaged mobility model was also run using the output from the wave resolved SWASH model using sliding filters to calculate the wave-averaged parameters. For skewness and acceleration either the sliding version filter of the model output was used, or the Ursell number ($U_r = 0.375\, H_s k/(kh)^3$) based parameterization of [11] with the same coefficients as XBeach were used. This allows comparison of the wave-averaged and wave resolved parametrized burial and mobility models with similar inputs, before comparing them with completely different hydrodynamics models.

4. Results and Discussion

4.1. Wave Resolved Methods

Swash Spectral Input: The initial comparison of the phased resolved and phase averaged results were performed with the SWASH nearshore hydrodynamics model run with the 2014 Martha's Vineyard field deployment bathymetry with constant wave height Jonswap spectral wave input. The spectral wave forcing allows group time scale variations in wave energy but keeps the energy constant at longer time scales. The model was run for 2 hours, and the offshore currents reached an equilibrium state after 1 hour. The 2nd hour of the run was copied and concatenated to create a 9-hour time series. The model was run with three different wave height inputs (1.5, 2 and 3.5 m) and five different initial locations at depths of (2, 3, 4, 5 and 6 m) corresponding to x-locations of (65, 107, 154, 199 and 239), where the mean water shoreline is at x=0 (Figure ES-6). The waves were turned on instantly at the beginning of the simulation and propagated across the domain. This rapid onset of high wave energy combined with the low density of UXO (*S* = 2.0) in the simulation allowed the UXO to be mobile at all times during the simulation. For a given wave height the UXO converged on a specific cross-shore location from the different initial locations within 2 to 3 hours. This location was determined by a balance of offshore forcing from mean currents (red lines in Figure ES-6, lower panel) and onshore forcing due to skewness (blue lines) and acceleration (green lines). The offshore mean currents extend to

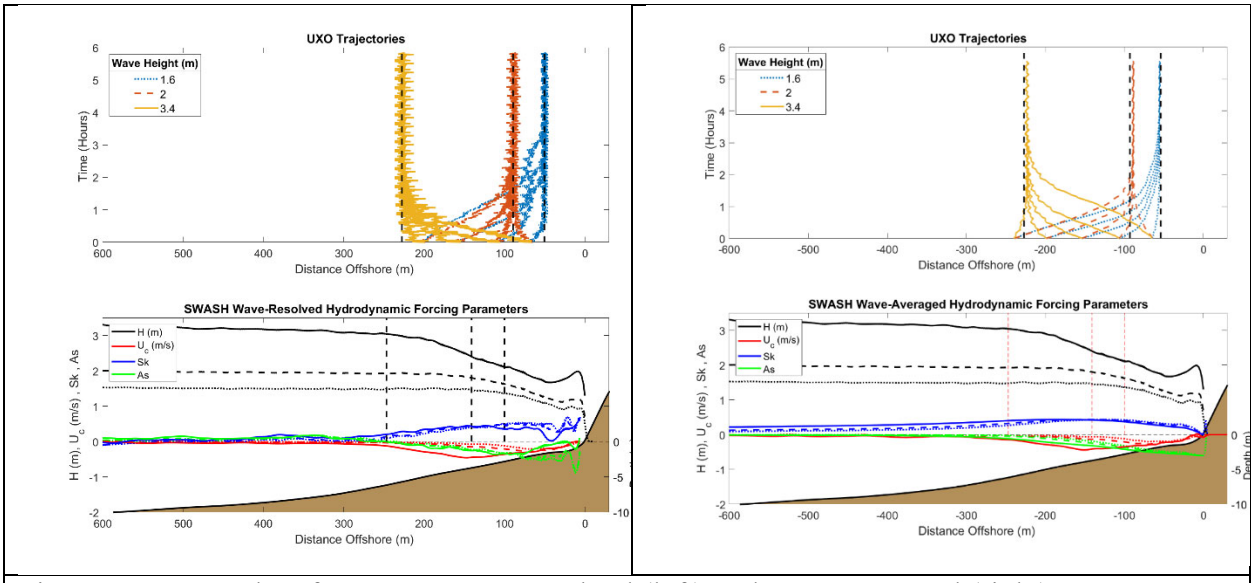

Figure ES-6. Results of SWASH wave-resolved (left) and wave-averaged (right) UXO mobility and burial modelling. Upper Panels) Time series of UXO migration paths for the three different wave heights and five different initial conditions. A power law location (x_{bp}) related to the breaking index is shown as the vertical black dashed lines. Lower Panels) Hydrodynamic forcing parameters including wave height (black), mean current (red) skewness (blue) and acceleration (green). The location (x_b) of the breaking point based on a breaker index is shown as the vertical black dashed lines.

the edge of the surf zone where wave height begins to decrease due to dissipation from breaking. The vertical dashed black lines depict the outer edge of the surf zone location (x_b) defined by a breaker index (γ_b) of wave height divided by depth (H/h) of 0.55. [12].

4.2. Wave Averaged Methods

To compare the phase resolved model to the phase averaged approach the output from the spectral input SWASH runs were phase averaged with a sliding window of $20Tp$ = 220 seconds and the input quantities from the interpolation function were calculated from these windowed sections. The same low relative density of S = 2.0 was used for these calculations. The *Sk* and *As* parameters were calculated from the Ursell number based approach discussed in section 3.2 (phase avergaed methods, main report), thus the input to the mobility and burial model has the same mean currents, but spatially smoother Sk and As input (Figure ES-6). The results are remarkably similar to the phase resolved models with less variation in UXO location on the wave and wave group time scale since some of this variability is averaged out with the sliding window calculations. In particular, the convergence location is almost the same as the previous method.

The UXO mobility model was also run using the output of the Xbeach model for the same initial UXO density, locations and spectral wave heights as the SWASH runs (results not shown in this summary). The results are similar to the SWASH results with object initiating near the beach migration offshore with the large wave case and object initiating offshore migration onshore with the small wave case. This suggests that the interpolation function is a suitable method for transitioning from a wave resolved to wave-averaged approach.

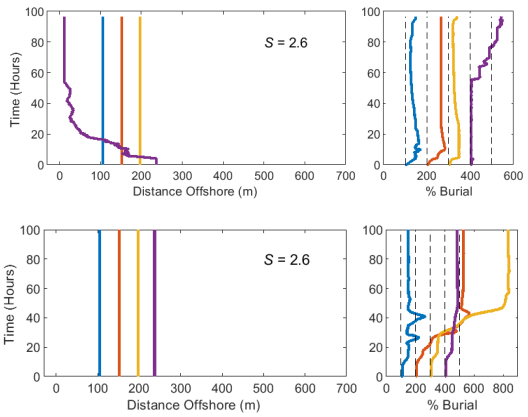

Figure ES-7. Comparison of Xbeach Wave-averaged UXO mobility post processing results with $\alpha = 0.25$ and $S = 2.6$ with morphology on for the 2014 measurements (upper panel) and 2018 measurements (lower panel). With the same parameters but different hydrodynamic forcing the model simulations show onshore mobility in 2014 followed by burial by sand bars and no mobility and deep burial due to migrating sand bars in 2018. The simulation results are consistent with measurements from both field deployments.

4.3. Simulation of Field Measurements

Both SWASH with the wave-averaged UXO mobility post-processing module and Xbeach were run with input from field observations taken during the 2014 and 2018 experiments on Martha's Vineyard. The initial locations ranged from x= 65 m offshore of the beach to 240

offshore of the beach corresponding to depth of 2 to 6 m. The center location of x = 150, D = 4 m is similar to the center of the field deployment locations. The SWASH results (not shown here) show more mobility than measured in the field since SWASH does not include burial by immigrating sand bars.

Results from the Xbeach simulations based on input forcing from both 2014 and 2018 data, with a specific set of input parameters of UXO relative density of $S = 2.6$ and the scaling parameter for the time dependence $\alpha = 0.25$, are shown in Figure ES-7. The simulations with forcing from the 2014 field experiment conditions show morphodynamic change in the form of accretion in the near shore part of the domain. This results in deep (150% of UXO Diameter) burial of an UXO that migrated from the furthest offshore initial condition to the accretion region. This onshore migration of some of the UXO is consistent with the 2014 measurements as shown in Figure ES-1. The simulations with forcing from the 2014 field experiment conditions show morphodynamic change in the form of offshore sand bar migration consistent with observations. Despite the larger wave height in 2018 the offshore migrating sand bars buried all UXO and results in no mobility (Figure ES-2). Two of UXO in the 2018 simulations were buried several diameters by the sand bars consistent with measurements.

5. Implications for Future Research/Implementation

The approach of using a wave-averaged nearshore hydrodynamics model with a parametrized mobility and burial post-processing model module that is derived from wave resolved simulations appears to have ability to hindcast observed UXO mobility and burial behavior from two different sets of observations with the correct choice of tuning parameters. The wave-averaged nearshore hydrodynamics model (in this case Xbeach) is computationally efficient and provides predictions of morphodynamic change which is essential for burial predictions. While there are many parameters that could be tuned, the mobility and burial post-

processing model is most sensitive to the parameter α, which scales the time constant on the non-equilibrium burial model. Selecting high values of this parameter results in burial that lags the predicted equilibrium scour and enhanced mobility. Low values result in similar prediction to the equilibrium burial model which typically predicts less mobility than observed. While the simulations with forcing based on measurements have complex time dependence due to time varying input, the simulations with constant wave height forcing generally suggest that low density UXO migrate in a similar manner to sand bars. In moderate wave energy conditions sand bars tend to migrate onshore due to weak undertows and breaking near the beach and in more energetic conditions the sand bars migrate offshore due wave breaking further offshore and stronger returns flow. Additional observations planned for 2023 with initial locations in a cross-shore distributed array will evaluate this hypothesis.

Future work to extend the approach to simulations resolving along and across-shore processes is relatively straight forward conceptually and would be useful to test if models can predict the lack of along-shore UXO migration observed in these data sets and make predictions about expected along-shore migration in locations with stronger along shore currents.

Since the wave-averaged hydrodynamic modelling combined with parameterized mobility and burial modelling approach is relatively computationally efficient it could provide a basis for monte-carlo simulations spanning a wide variety of input parameters for input into statistical models such as UnMES (Underwater Munitions Expert System [13])

References:

[1] P. Traykovski, "MR-2319: Continuous Monitoring of Mobility, Burial and Re-Exposure of Underwater Munitions in Energetic Near-Shore Environments." [Online]. Available: https://www.serdp-estcp.org/Program-Areas/Munitions-Response/Munitions-Underwater/MR-2319/MR-2319/(language)/eng-US.

[2] P. Traykovski, "MR-2729 Rapid Response Surveys of Mobility, Burial and Re-exposure of Underwater Munitions in Energetic Surf-Zone Environments and Object Monitoring Technology Development," 2020. [Online]. Available: https://www.serdp-estcp.org/Program-Areas/Munitions-Response/Munitions-Underwater/MR-2729/MR-2729/(language)/eng-US.

[3] J. Calantoni, T. Staples, A. Sheremet, and U.S. Naval Research Laboratory, "Long time series measurements of munitions mobility in the wave-current boundary layer," U.S. Naval Research Laboratory, Mar. 2014.

[4] S. E. Rennie, A. Brandt, and C. T. Friedrichs, "Initiation of motion and scour burial of objects underwater," *Ocean Eng.*, vol. 131, pp. 282–294, Feb. 2017.

[5] C. Friedrichs, S. E. Rennie, and A. Brandt, "Self-burial of objects on sandy beds by wave- and current-induced scour," 2016.

[6] Y. A. Cataño-Lopera and M. H. García, "Geometry of scour hole around, and the influence of the angle of attack on the burial of finite cylinders under combined flows," *Ocean Eng.*, vol. 34, no. 5, pp. 856–869, Apr. 2007.

[7] P. Nielsen, *Coastal Bottom Boundary Layers and Sediment Transport*. World Scientific, 1992.

[8] R. Whitehouse, *Scour at Marine Structures: A Manual for Practical Applications*. Thomas Telford, 1998.

[9] P. Traykovski, "Observations of wave orbital scale ripples and a nonequilibrium time-dependent model," *J. Geophys. Res. C: Oceans*, vol. 112, no. C6, 2007.

[10] E. Meyer-Peter and R. Müller, "Formulas for bed-load transport," *IAHSR 2nd meeting, Stockholm*, 1948.

[11] B. G. Ruessink, G. Ramaekers, and L. C. van Rijn, "On the parameterization of the free-stream non-linear wave orbital motion in nearshore morphodynamic models," *Coast. Eng.*, vol. 65, pp. 56–63, Jul. 2012.

[12] Y. Goda, "Reanalysis of Regular and Random Breaking Wave Statistics," *Coast. Eng. J.*, vol. 52, no. 1, pp. 71–106, Mar. 2010.

[13] S. Rennie and Johns Hopkins Applied Physics Laboratory Baltimore United States, "Underwater munitions expert system to predict mobility and burial," Johns Hopkins Applied Physics Laboratory Baltimore United States, Nov. 2017.

Final Report

Table of Contents

List of Figures

Acronyms

MRSEED	Munitions Response Exploratory Development Solicitation
MRSON	Munitions Response Statement of Need
SERDP	Strategic Environmental Research and Development Program
sUXO	Surrogate Unexploded Ordnance
SWAN	Shallow WAves Nearshore hydrodynamics model
SWASH	Simulating WAves till SHore hydrodynamics model
UXO	Unexploded Ordnance
WHOI	Woods Hole Oceanographic Institution

Abstract

Objective

One of the critical areas for underwater munition detection and remediation is very shallow water less than 5 m deep. The very shallow water emphasis comes from the fact that munitions are most likely to be encountered by the general public in depths that are suitable for wading, swimming, and scuba diving, with potential encounters more likely in the shallowest water. In many environments there will be occasional to frequent breaking waves in depths from 0.5 m to 3 m. In this region Unexploded Ordnances (UXO) may either bury, remain proud of the seafloor, or become re-exposed. In environments with energetic forcing or steep slopes the UXO may migrate. Numerical modelling of environmental conditions and UXO response is a powerful tool to assess the relative likelihood of these processes. The overall objective of the work was to improve models for hydrodynamic forcing of UXO migration and burial in shallow water surf-zone environments. Our work addressed the following questions:

- Does the balance between onshore forcing by wave asymmetry and skewness and offshore forcing by return flows control mobile UXO location in the surf-zone?
- Are the wave asymmetry, skewness and return flow processes in the surf zone represented by phase averaged models adequately to reproduce observed UXO migration events?
- What is the role of morphology (e.g., migration of sandbars) in UXO burial and migration and can this be captured by phase resolving models?

Technical Approach

The research used both a wave-resolving model (SWASH) that explicitly computes non-linear wave transformations and a wave-averaged model (XBeach) that parametrizes nonlinear transformations in terms of wave asymmetry and skewness. The output of these nearshore hydrodynamic models is input into a parameterized UXO burial and mobility post-processing module based on a previously developed time-dependent burial model. Our approach investigated the balance between onshore forcing by wave asymmetry and skewness and offshore forcing by return flows as described by an interpolation function calculated from the parameterized equations of motion for a cylinder. The advantage of the wave-averaged models is three-fold. First, wave-averaged models have a much lower computational expense allowing rapid modelling of larger operational areas. Second, Due to the lower computation expense longer runs which capture coastal morphodynamic change are possible. Third, wave-averaged models can span a wider parameter space and are useful for developing ensemble results for inclusion in statistical models of munitions behavior.

Results and Benefits

When forced with steady waves both phase-averaged and resolved models show similar results of low density (S = UXO density / Water density < 2.5) UXO migration towards the outer edge of the surf zone where offshore returns flows balance onshore forcing due to skewness and acceleration in the absence of burial by migrating sandbars which were only modelled with the phase averaged model. The location of the balance point can be calculated by a power law relation with the breaker index (Wave Height divided by Water Depth) for inclusion in probabilistic models for UXO migration. The time dependent model typically predicts burial of higher density (S > 3.5) UXO. In the transitional regime (2.5 > S > 3.5) the threshold for mobility depends on the rate of wave energy increase. If a proud UXO is suddenly forced with large waves it is more likely to migrate than a UXO that is forced with moderate waves for prolonged periods allowing scour burial. When forced with time series of wave conditions from two different field deployments the modelling system produced output of deep burial by offshore migrating sand bars in one case and onshore migration of low density UXO in the other, consistent with

measurements.

Our work is in response to the fiscal year 2021 Statement of Need for the Munitions Response Program Area (MRSON-21-S1). The models can aid management of UXO by improving understanding of the potential for UXO migration during the time between wide area surveys, detailed surveys, and removal of UXO by divers. The models can improve site managers' capabilities to prioritize sites where UXO are most likely to move into public or populated areas.

.

1. Objectives

The objectives of the work were to develop and evaluate a suite of modeling approaches to describe UXO migration trajectories in the surf zone. These models combined with observations from previous studies will be used to **assess a conceptual hypothesis that the balance between onshore forcing by wave skewness and asymmetry and offshore return flows controls the location of mobile UXO in the surf zone**. A wide range of models are available for surf zone hydrodynamics ranging from wave-averaged models such as DELFT3D coupled with SWAN, to short wave-averaged and long wave (infragravity) resolving models such as XBeach, to wave resolved models such as SWASH. In order to predict on and offshore sand bar migration, the wave-averaged models have parametrized descriptions of wave skewness (*Sk*) and asymmetry (*As*), while the wave resolving models explicitly calculate the non-linear wave transformations that control *Sk* and *As*. All of these models resolve the offshore return flows, but have significant differences, due to vertical resolution and wave driven flow formulations. **Thus, a second objective of the proposed work was to determine if the parametrized calculations of *Sk* and *As* in the wave-averaged models are sufficient to predict on and offshore migration, and the final deposition zones of UXO in the surf zone.** The second objective will be addressed by evaluating the results of the wave-averaged models relative to wave resolving modes and observations.

The third objective was to evaluate the potential of using wave-averaged models with a wide range of input parameters to develop databases for statistical models. The motivation for a one-year MRSEED proposal as opposed to a larger effort was that it was not known a-priori without conducting the research whether the wave-averaged models will be accurate enough to achieve this third objective. One of the important results of the research is that the parametrized calculations of *Sk* and *As* in the wave-averaged models were sufficiently accurate to hindcast field observations of UXO mobility forced by non-linear wave processes.

2. Background

Recent field measurements (MR2319 & 2729, Traykovski [1], [2] and MR2320, Calantoni [3]) of the mobility, burial and re-exposure of munitions have significantly increased our knowledge of the parameters that control mobility and burial. The measurements in MR2319 conducted on the South Shore of Martha's Vineyard, MA indicate that medium sized (D = 7 and 15 cm, L = 75 cm) low density surrogate UXO ($\rho_0 < 2.5$ g/cm^3) were observed to migrate up to 160 m onshore, across the surf zone, while denser objects buried in place in response to waves with 2.5 m significant wave height (H_s).

In contrast, in a more recent field deployment conducted in winter of 2018 (MR2729) at the same location with similar surrogate UXO, but much larger waves (H_s = 3.5 m), little to no large-scale onshore migration was measured despite the more energetic forcing and evidence of small-scale object mobility. In the more recent deployment, while the surrogate UXO did not migrate the sand bar migrated from a location near the beach to the location where the UXO

were deployed in 3 to 4 m water depth, burying the UXO in up to 1.5 m of sand.

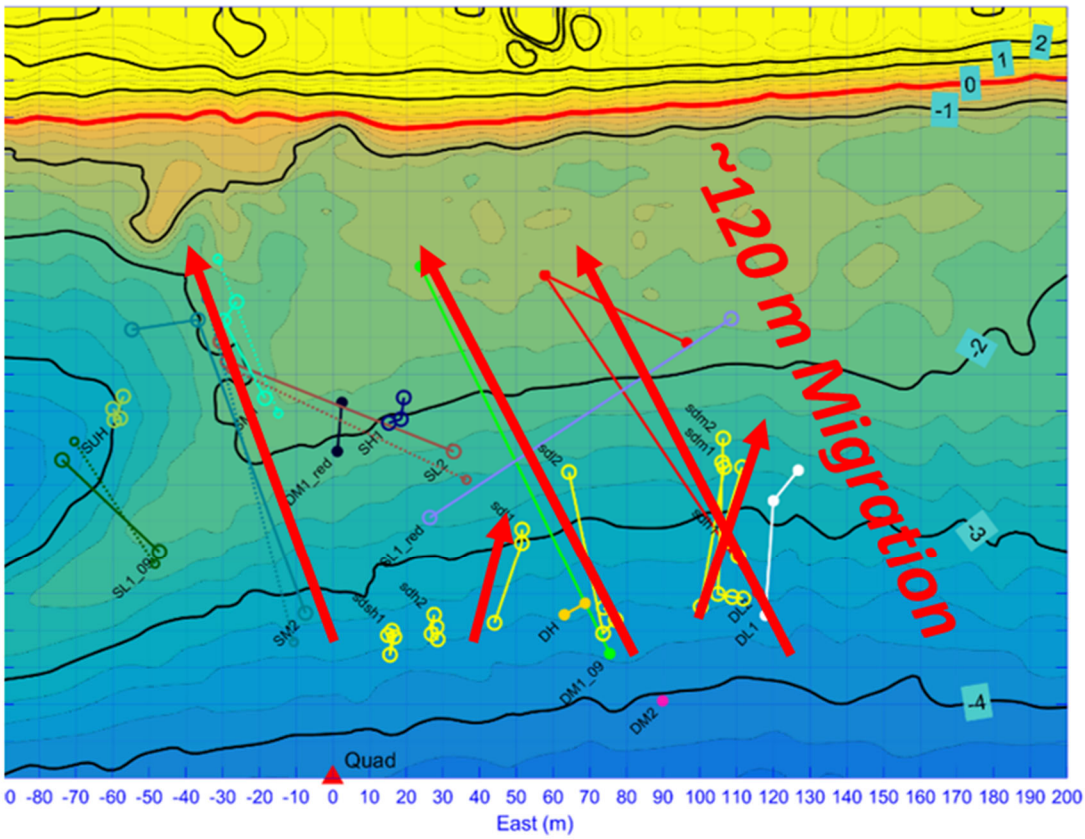

Figure 1. Top Panel) Bathymetry and UXO migration path from MR2319 in 2014 on the south coast of Martha's Vineyard. Bottom Panel) Wave Height time series

To help understand the physical mechanisms that led to onshore migration in moderate height waves and no migration with larger waves as part of MR2729, the output from a wave resolving numerical model for surf-zone hydrodynamics (SWASH) was coupled with a post-processing module that includes the equation of motion for a cylindrical UXO (*Object mobility* described below) and parametrization of the time dependent burial by wave induced scour (*Object Burial* described below).

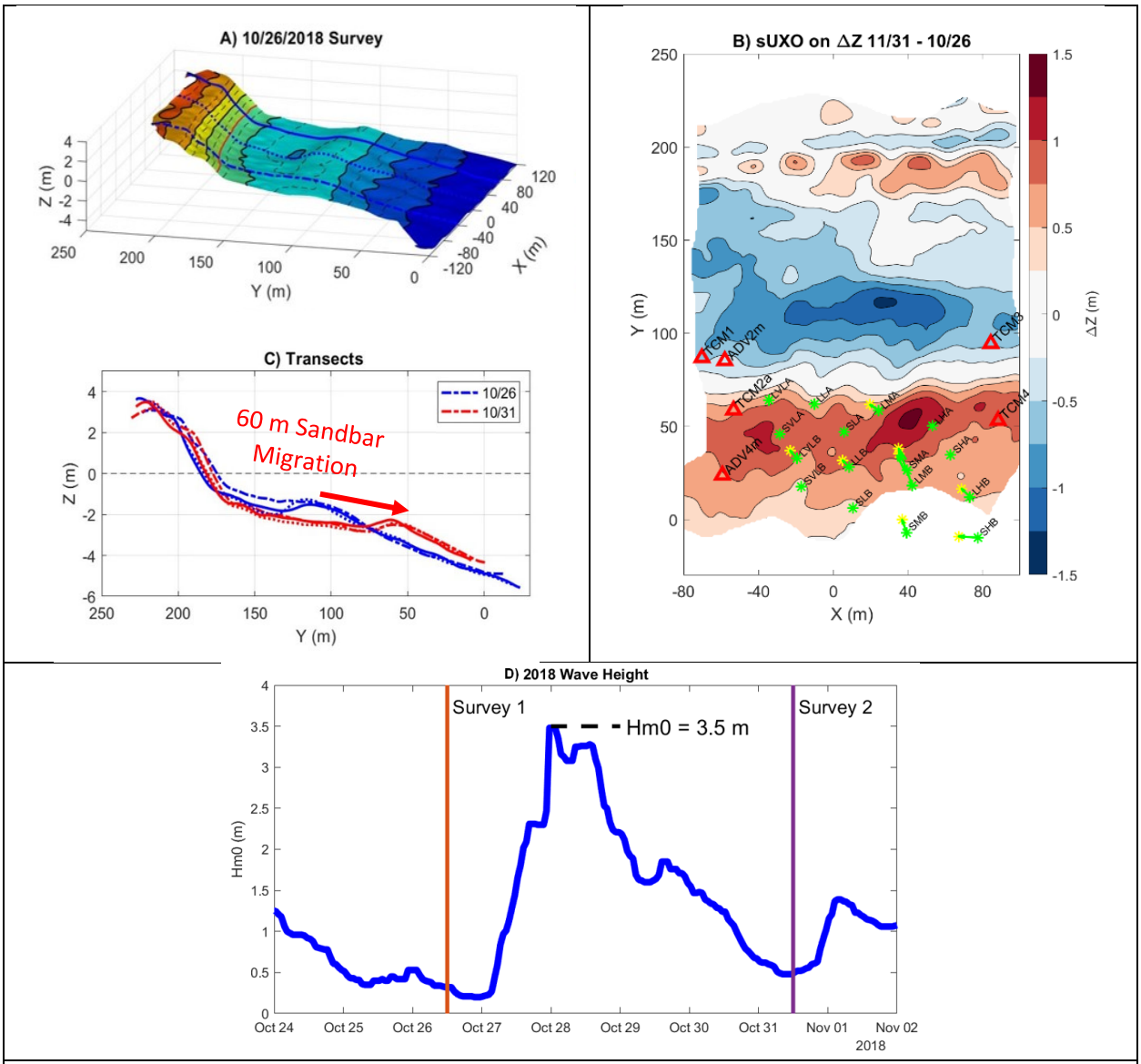

Figure 2. A) Initial Bathymetry from MR-2729 in 2018 on the south coast of Martha's Vineyard. B) Bathymetric change map and sUXO migration paths. C) Transects as shown in A. D) Wave Height time series

Object Mobility: The parameter space where burial versus migration is expected can be examined by considering the moments on an object resting on a deformable sand bed (Figure 3 In a highly simplified analysis, the moment per unit length that will induce roll of the cylinder is

$$T_f = FD_o(1/2 - p_b), \tag{9}$$

where D_o is the diameter of the object, p_b is the fractional burial and is related to the depth of burial (b_d) by $p_b = b_d/D_o$. The total lateral force (F) on the object consists of the sum of three terms, the drag force (F_D), the inertial force (F_I) and the pressure gradient force (F_P),

$$F = F_D + F_I + F_P. \tag{10}$$

The drag force due to water motion (U) is

$$F_D = \rho_w C_d U|U| D_o/2, \tag{11}$$

the inertial term is

$$F_I = C_m \rho_w \pi D_o^2 \dot{U}/4, \tag{12}$$

and the pressure gradient term is

$$F_P = \rho_w \pi D_o^2 \dot{U}/4. \tag{13}$$

C_d and C_m are the drag and inertial coefficients. ρ_w is the water density. $\dot{U}$ is the flow acceleration. The stabilizing moment caused by the weight of the cylinder per unit length when the object is less than halfway buried is $T_w = WD_0\sqrt{p_b(1/2 - p_b)}$, based on a submerged weight of

$$W = \cos(\beta)(\rho_0 - \rho_w) g \pi D_0^2/4\,, \tag{14}$$

where ρ_0 is the object density and β is the seafloor slope. The ratio of the destabilizing forces due to drag only and the stabilizing forces is quantified by the object Shields parameter (θ_{op_b}) based on percent burial ($p_b = b_d/D_o$) on a flat seafloor are:

$$\theta_{op_b} = \frac{C_d U|U|^2}{g(S_o - 1)D_0} \frac{2(1/2 - p_b)}{\pi\sqrt{p_b(1/2 - p_b)}} = \theta_o \frac{2(1/2 - p_b)}{\pi\sqrt{p_b(1/2 - p_b)}} \tag{15}$$

The key parameters in this expression are the diameter of the object and the initial depth of burial as these determine the moment arms, and the current velocity (U) combined with the relative density of the object (S_o) as these determine the forces.

A similar analysis on a grain of sand with median diameter (d_{50}) results in the Shields criteria for initiation of sand motion [4] . The Shields parameter based on percent burial (θ_{op_b}) can be expressed as the Shields parameter from sediment transport theory θ_o and a geometric initial burial term, which is similar to a frictional coefficient. This geometric term only accounts for the relative lever arms in the torque balance and not in the reduction in exposed diameter for the drag term and reduction in area for the inertial and pressure gradient terms due to burial. At low values of p_b the difference is small but does become significant as the object becomes buried further.

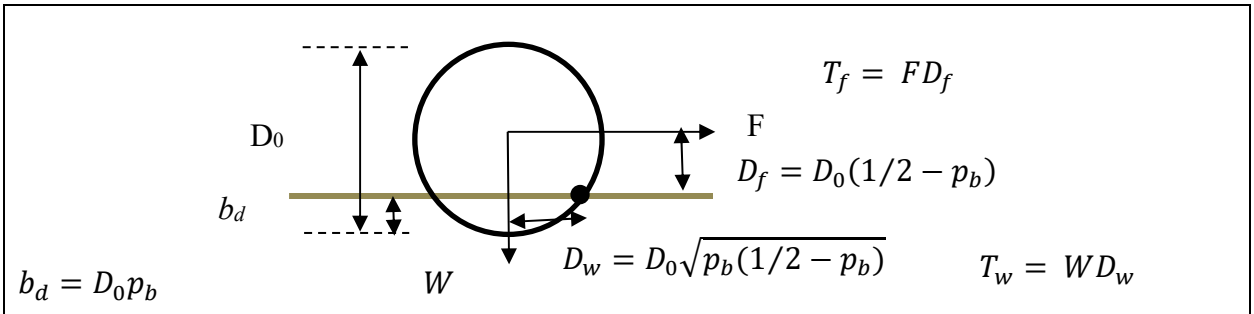

Figure 3. Schematic of torque balance ($T_f = T_w$) about the tipping point shown as a black dot on a cylindrical UXO.

These calculations assume a stationary object and thus are used to calculate thresholds of initial motion. For a dynamic analysis to calculate migration rate and distance, the water

velocity can be replaced by the relative velocity between the water and the object (U-U_0). The acceleration of the object can be calculated from a force balance

$$\frac{\rho_0 \pi D_o^2 \dot{U}_o}{4} = F - \mu W + F_g \tag{16}$$

Where the friction coefficient is given by

.

$$\mu = \sqrt{p_b(1/2 - p_b)}/(1/2 - p_b) \tag{17}$$

The downslope gravitational term (F_g) is given by

$$F_g = \sin(\beta)(\rho_o - \rho_w) g \, \pi D_o^2/4 \tag{18}$$

These dynamic calculations require the full phase resolved series of water velocity as the shape of the wave is important for correctly calculating the flow acceleration ($\dot{U}$). The migration distance of the object (X) can be found by integrating the object acceleration in Eqn 8.

$$X = \iint \dot{U}_0 dt \, . \tag{19}$$

Object Burial: Laboratory data and some field data have also been used to develop parameterized expressions for the state of burial of cylinders, mines, and ordnance-shaped objects. There is a large body of literature on this subject and the results are well summarized in Rennie, Friedrichs, and Brandt [5][6] (henceforth referred to as RBF16). This work suggests the following expression for equilibrium burial depth:

$$p_{b,eq} = a_2 \theta_{sed}^{b_2} a_2 \Theta_{sed}^{b_2} a_{KC} KC^{b_{KC}} \tag{20}$$

The values proposed by Y. A. Cataño-Lopera and M. H. García [7] of a_2 = 1.6 and b_2 =0.85 for wave periods of T > 4 s were used for predictions of burial depth in this study. The parameter a_{KC} was set 0.1 and b_{KC} was set to 0.51. The sediment Shields parameter is calculated from

$$\theta_{sed} = \frac{f_w U_{br}^2}{g(S_o - 1) d_{50}} \tag{21}$$

where the wave friction factor (f_w) is based on the expression from Nielsen [8]:

$$f_w = \exp\left(5.5 \left(\frac{12 U_{br} T_p}{2\pi d_{50}}\right)^{-0.2} - 6.3\right) \tag{22}$$

U_{br} is the near bed wave orbital velocity and T_p is the peak wave period.
The equilibrium burial depth formulations relate the final depth of burial to constant wave forcing conditions. The burial process is known to take a finite amount of time, which is related to the sediment transport rate and the size of the scour pit that the object will self-bury in.

Whitehouse et al. [9] modeled time-dependent burial as a logistic process, whereby the burial depth (p_b) follows the equilibrium burial depth ($p_{b,eq}$) with a timescale (T^*):

$$\frac{dp_b}{dt} = \frac{p_{b,eq} - p_b}{T^*} \tag{23}$$

This expression is similar to that used by Traykovski [10] for modeling time-dependent evolution ripple geometry. For a step change in forcing, this results in the following:

$$p_b(t) = p_{b,eq}\left(1 - \exp\left(-\frac{t}{T^*}\right)\right) \tag{24}$$

The timescale is the ratio of the object diameter squared to the sediment transport rate:

$$T^* = \frac{\alpha\theta_{sed}^N D_o^2}{(g(S_{sed} - 1)d_{50}^3)^{0.5}} \tag{25}$$

The parameter N is set to 1.5 based on the Meyer-Peter Müller [11] sediment transport rate

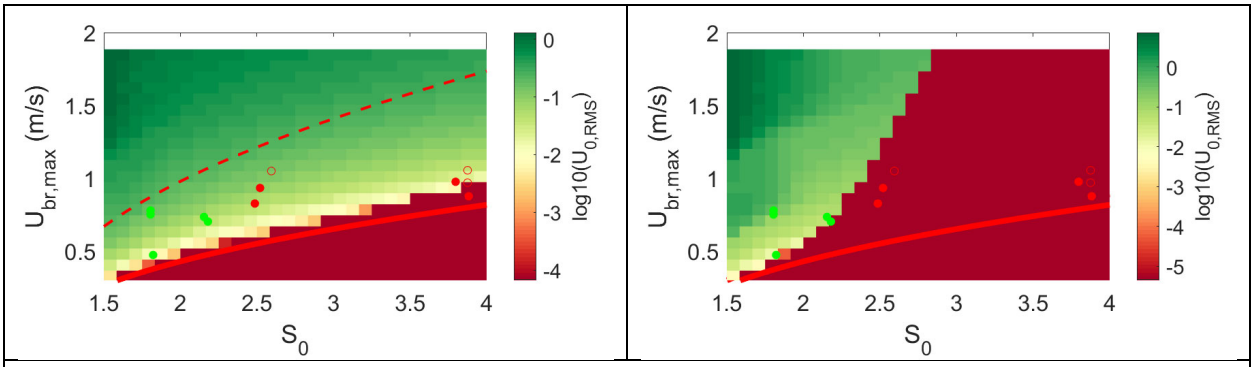

Figure 4. Results of the UXO migration model developed in MR2729 for (left) a constant 5% (solid red line) and 30% (dashed red line) burial depth case and (b) time dependent scour case. The red lines are thresholds predicted from methods described in RBF16 and the red and green dots are measurements of UXO migration from MR2719, in which the green dots indicate object that migrated, and the red dots indicate stationary objects.

formulation, and the parameter α is used to tune the model to field data sets. The mobility thresholds calculated by the RBF16 method and equations 1 and 2 were compared to measurements of surrogate UXO mobility as described in the MR2719 final report. When these methods were used to calculate thresholds based on a time invariant initial burial depth of 10% the model failed to segregate the data into mobile and non-mobile classes (Figure 4, left). The model was run with 5% and 30% initial burial. The model predictions are shown as a color plot of UXO root-mean-squared velocity ($U_{0,RMS}$) versus UXO relative density (S_0) and wave forcing velocity (U_w). The transition from red (stationary) to green (mobile) in the color plot compares well to the red line predicted by the RBF16 method. The methods described in the MR2319 final report and in RBF16 only predict the thresholds of mobility and are not able to predict migration rates. The method developed in MR2729 and described here predicts both the threshold and migration rates, and the threshold predictions are consistent with the previous methods. Points above the curve are predicted to be mobile (green zone for p_b = 5%), and points below (red zone for p_b = 5%) are predicted to be stationary. The observations are plotted as green points in (U_{br}, S_0) space for mobile objects and red points for stationary objects. Both predictions for p_b of 5%

(red line) and 30% (dashed red line) are inconsistent with the observations of UXO mobility. A mobility threshold curve based on an initial state of burial of 5 % incorrectly predicts that all objects, including those with S_o greater than 2.5, would be mobile. A threshold curve based on an initial state of burial of 30% incorrectly predicts that all objects, including those with S_o less than 2.5, would be stationary. Curves between 5% and 30% do not result in better predictions because the theory does not account for the dramatic change in mobility/burial behavior near a relative density of 2.2 to 2.6, which is slightly above the typical density of 2.0 for water-saturated sand beds.

As described in the MR2719 final report, since the burial process is known to be a time-dependent process, it is not physically realistic to assume a constant initial burial of some predetermined value. The threshold for mobility of objects on a mobile bed is likely to be set by the rate of burial relative to the rate of wave energy increase. If an initially proud object is instantaneously subjected to wave forcing greater than the threshold of motion, it will move before it has time to bury. If the wave forcing is increased very slowly with rates much slower than the timescale for burial, the object will become sufficiently buried with a burial depth given by the equilibrium burial depth (Eqn. (20)), so it will not move unless the entire bed is fluidized, which requires extremely high wave energy or strong pressure gradients. In the MR2319 final report, a method is described that couples the RBF16 wave-averaged mobility thresholds with the time dependent burial equations. This previous method can predict initiation of motion but cannot predict migration rates. In the new work conducted as part of MR2729 we coupled the wave-averaged burial model with a wave phase resolved mobility model that allows predictions of both mobility thresholds and migration rates. The initiation of motion results of this model are similar to those presented in figure 34 of the MR2319 final report. These time-dependent mobility curves show quite different behavior than either the fixed burial depth curves or the equilibrium burial depth curves. Initially, when the waves are small, the mobility threshold curve follows the curve based on the initial burial of 5% (Figure 4, right). Depending on dU_{br}/dt, at some later time, the objects rapidly bury and are no longer mobile. For Figure 4 (right panel) the wave amplitude is linearly increased with time over a period of 2 hours from zero to a value of $U_{br,max}$ that is varied to change the rate of wave energy increase. With increasing values of dU_{br}/dt or increasing values of the parameter α in the time scale term (T^*) this occurs at higher value of S_o. The time-dependent mobility predictions with $\alpha = 0.5$ successfully segregates the data into mobile and stationary categories, roughly consistent with the data, although some of the points are very close to the threshold (Figure 4, right). Note that the y-axis of Figure 4 is the maximum velocity at the end of the linearly increasing wave amplitude time series (U) and not the exact orbital velocity at the object begins to move. A figure where the y-axis is transformed via interpolation and binning into the exact velocity at initiation of motion ($U_{br,i}$) is shown in Figure 5. The method of displaying the results shows increased dependence on density with a threshold at a constant density depending on the parameter α. Most of this background work was conducted as part of MR2729 with some additional testing and refinement of the code into functions for burial and mobility in MR21-1341, which will be described in the next section.

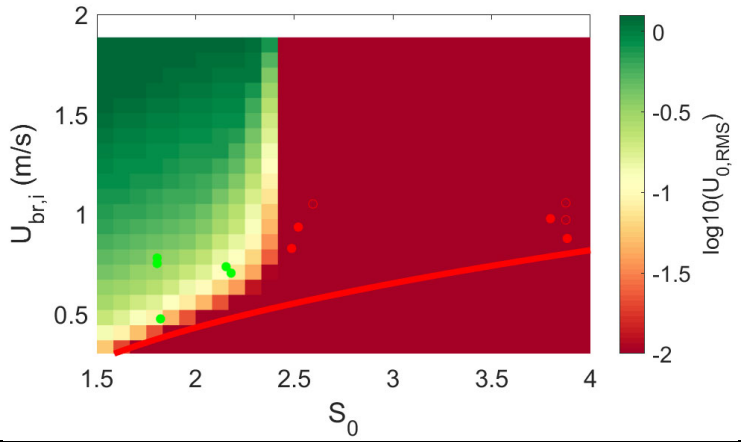

Figure 5. Thershold of mobility as a function of density with $U_{br,i}$ on the y-axis

3. Materials and Methods

3.1. Phase resolved methods

The new methods developed in MR21-1341 begin with refinements to the wave resolved mobility and burial model. The first step was to break the burial and mobility into separate functions so the same function can be used in a variety of applications. Equations (1) through (9) were incorporated in the CylForceBalance.m function which updates the UXO velocity for the next time step ($U_{0,t+1}$) based on inputs of (g, β, p_b, C_d, ρ_w, ρ_o, D_o, U, $\dot{U}$, $U_{o,t}$, Δt). An additional modification was added to Equation 8, whereby the friction coefficient was modified ($\acute{\mu} = \mu U_o/|U_o|$) so that force of friction is in the opposite direction of the UXO velocity if the UXO is mobile and in the opposite direction of the hydrodynamics forces ($\acute{\mu} = \mu F/|F|$) if the UXO is stationary. A second check was also performed to ensure the frictional force could stop the motion of the UXO, but not reverse the motion:

$$if\ |\mu W| > |F|\ \&\ (U_{o,t+1} * U_{o,t}) \leq 0\ then\ U_{o,t+1} = 0 \tag{26}$$

The time dependent burial formulation (Equations 10 through 15) were incorporated into a second function, BurialUpdate.m which outputs the updated time dependent burial depth and equilibrium burial depth ($p_{b,t+1}, p_{b,eq}$) based in the inputs of (g, ρ_w, ρ_o, D_o, U_{br}, T_p, d_{50}, α, $p_{b,t}$, $p_{b,min}$, $U_{o,t}$, Δt). A minimum burial of $p_{b,min} = 0.05$ is assigned so the UXO always has some deformable bed rolling friction and this was typically used as the initial condition also. A key addition to the burial module for field data sets which have variations in wave energy that may bury or unbury UXO was a relation between mobility and unburial. For now, this is calculated by resetting the burial depth to $p_{b,min}$ if the UXO moves a fraction of the UXO diameter in a quarter wave period:

$$if\ |U_o| > 0.1\ \frac{D_o}{T_p/4}\ then\ p_b = p_{b,min} \tag{27}$$

A schematic of the overall computational flow chart is shown in Figure 6.

The phase resolved burial and mobility model described in the schematic can be forced with the bottom bin of the water velocity output (U_{br}, T_p, $U, \dot{U} = f(U_b(x_o, t))$) from a phase resolving nearshore hydrodynamics model such as SWASH, or spatially uniform input water velocity data can be generated to span a wide range of input parameters.

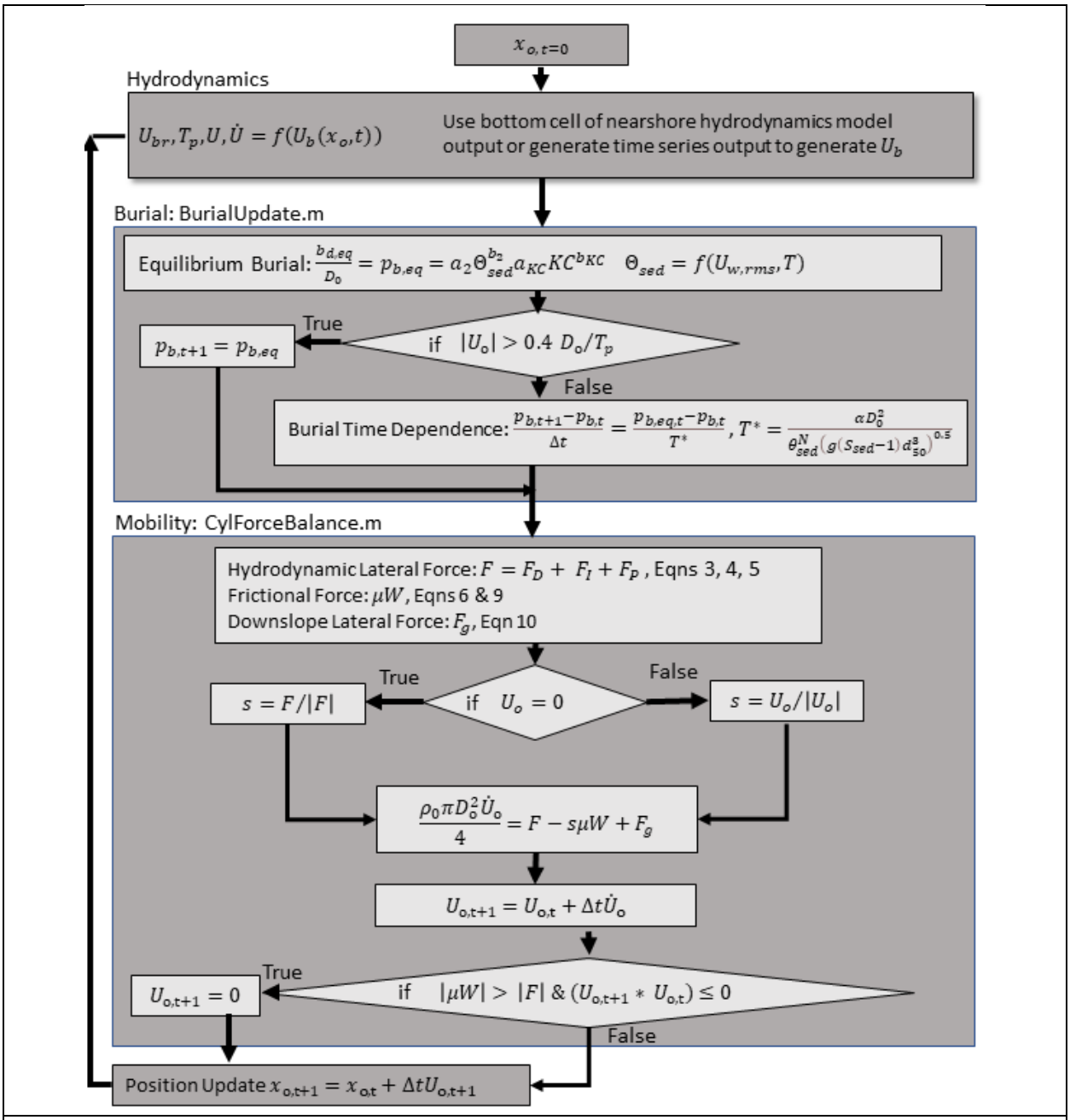

Figure 6. Computational flow chart for the parametrized wave phase resolved mobility and burial model

3.2. Phase averaged methods

In order to use the burial and mobility model with output from phase averaged models that only output variables such as U_{br}, T_p and U_c (the mean current velocity) and do not resolve the phase resolved quantities $U, \dot{U}$ the phase resolved model was run over a wide range of spatially uniform input parameters to develop a function that can be used to calculate the UXO velocity as a function of these parameters:

$$U_o = f_M(\rho_o, b_d, U_{br}, T_p, U_c, Sk, As, \beta) \tag{28}$$

A Matlab script was developed to loop over 7 to 17 steps for each parameter and run for all possible combinations of parameters and output results into an 8-dimensional matrix. The UXO diameter (D) was set at 0.15 m and the length (L) was set at 0.75 cm, but these parameters could easily be changed. UXO density (ρ_o), burial depth (b_d), representative wave orbital velocity (U_{br}) and seabed slope (β) were simply assigned values in the loop iterations. It is assumed that the burial depth does not vary over the short time scale of the input time series used to generate to the interpolation function but could change over the time step of the phase averaged hydrodynamics model. Combined wave (U_w) and current (U_c) velocity time series were calculated by $U = U_c + U_w$: where the wave terms is defined by

$$U_w = U_{br}\left(\sin(\omega t) + \frac{r\sin(\phi)}{1+\sqrt{1-r^2}}\right)/(1 - r\cos(\omega t + \phi)) \tag{29}$$

based on [12]. The parameters r and ϕ control the shape of the wave and were varied from 0.0 to 0.9 and $-\pi/2$ to $\pi/2$ respectively to span the entire range of values of *Sk* (0 to 1.6) and *As* (-1.6 to 0) found in field environments and predicted by the nearshore hydrodynamics models. The skewness and asymmetry are calculated from the wave component of the velocity time series as

$$S_k = \frac{\overline{(U_w^3)}}{\sigma_{U_w}^3}, \quad A_s = \frac{\overline{(H(U_w)^3)}}{\sigma_{H(U_w)}^3}, \tag{30}$$

where σ_{U_w} is the rms of near bed wave orbital velocity, and $H(U_w)$ is the Hilbert transform of U_w.

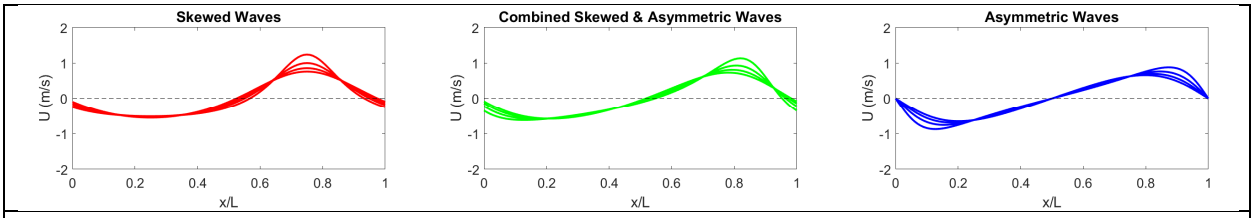

Figure 7. Wave shape of shoaling waves. left-skewed, middle combined skewness and acceleration, right acceleration only.

The results for predicted UXO velocity from the interpolation function evaluated over a range of U_{br}, Sk and U_{br}, As are shown in Figure 8.

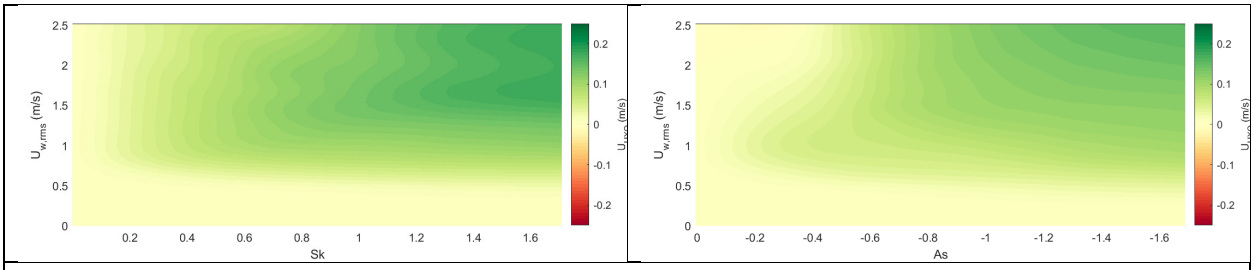

Figure 8. Predicted UXO velocity from the interpolation function evaluated over a range of U_{br}, Sk (left) and U_{br}, As (right).

The computational workflow for the wave-averaged model is similar to phase resolved model except instead of using the full equations of motion for UXO migration velocity the interpolation function is used and the input is from a wave-averaged nearshore hydrodynamics model such as XBeach. A simplified schematic of the workflow is shown in Figure 9.

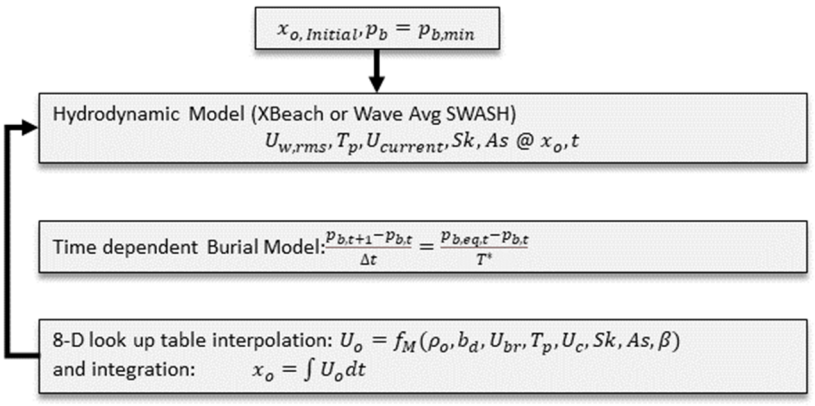

Figure 9. Comptutational flow chart for the parametrized wave phase averaged mobily and burial model.

For testing purposes, the wave-averaged mobility model was also run using the output from the wave resolved SWASH model using sliding filters to calculate the wave-averaged parameters. For skewness and acceleration either the sliding version filter of Eqn (30 was used, or the Ursell number ($U_r = 0.375\, H_s k/(kh)^3$) based parameterization of [13] with the same coefficients as XBeach were used. This allows comparison of the wave-averaged and wave resolved parametrized burial and mobility models with similar inputs, before comparing them with completely different hydrodynamics models.

4. Results and Discussion

4.1. Phase resolved methods

4.1.1. SWASH Spectral Input

The initial comparison of the phased resolved and phase averaged results were performed with the SWASH nearshore hydrodynamics model run with the 2014 Martha's Vineyard field deployment bathymetry with constant wave height Jonswap spectral wave input. The spectral wave forcing allows group time scale variations in wave energy but keeps the energy constant at longer time scales. The model was run for 2 hours, and the offshore currents reached an equilibrium state after 1 hour. The 2nd hour of the run was copied and concatenated to create a 9-hour time series. The model was run with three different wave height inputs (1.5, 2 and 3.5 m) and five different initial locations at depths of (2, 3, 4, 5 and 6 m) corresponding to x-locations of (65, 107, 154, 199 and 239), where the mean water shoreline is at x=0 (Figure 10). The waves were turned on instantly at the beginning of the simulation and propagated across the domain. This rapid onset of high wave energy combined with the low density of UXO (S = 2.0) in the simulation allowed the UXO to be mobile at all times during the simulation. For a given wave height the UXO converged on a specific cross-shore location from the different initial locations within 2 to 3 hours. This location was determined by a balance of offshore forcing from mean currents (red lines in Figure 10, lower panel) and onshore forcing due to skewness (blue lines)

and acceleration (green lines). The offshore mean currents extend to the edge of the surf zone where wave height begins to decrease due to dissipation from breaking. The vertical dashed red lines depict the outer edge of the surf zone defined by a breaker index (γ_b) of wave height divided by depth (H/h) of 0.55. [14].

$$\gamma_b(x_b) = 0.55 \tag{31}$$

Where x_b is the location that satisfies the equality in (31).

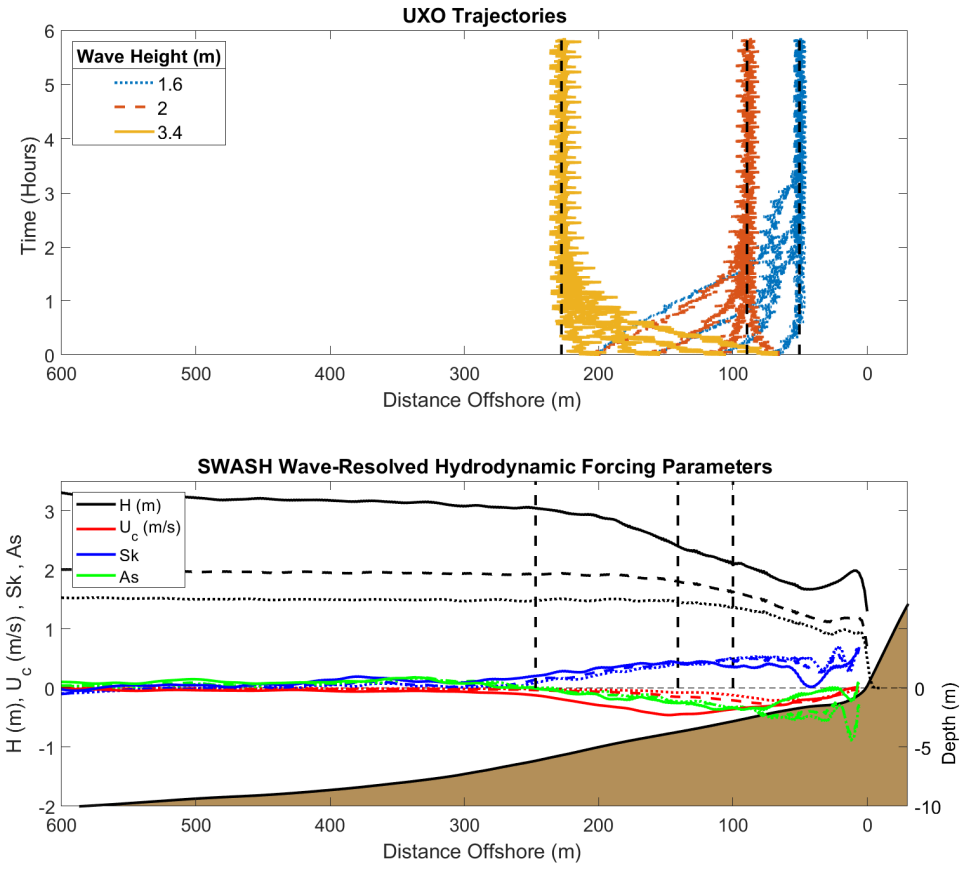

Figure 10. Results of SWASH wave resolved UXO mobility and burial modelling. Upper Panel) Time series of UXO migration paths for the three different wave heights and five different initial conditions. A power law location (x_{bp}) related to the breaking index is shown as the vertical black dashed lines. Lower Panel) Hydrodynamic forcing parameters including wave height (black), mean current (red) skewness (blue) and acceleration (green). The location (x_b) of the breaking point based on a breaker index is shown as the vertical black dashed lines.

The location of the UXO convergence (black dashed lines in Figure 10, upper panel) can be related to the γ_b location by a power law of

$$x_{bp} = bx_b^m \tag{32}$$

where the values b = 0.0236 and m = 1.66 result in the best fit to the model output for the phase resolved SWASH runs (Figure 11).

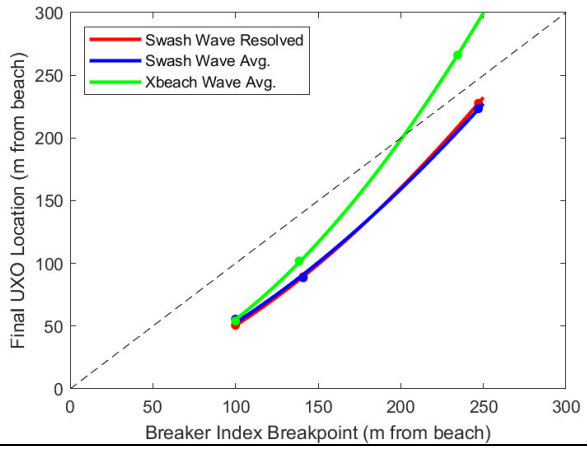

Figure 11. Predicted UXO final location vs Breaker Index Break point for the three different modeling approaches

4.2. Phase averaged methods

4.2.1. SWASH Spectral Input

To compare the phase resolved model to the phase averaged approach the output from the spectral input SWASH runs were phase averaged with a sliding window of $20t_h$ = 220 seconds and the input quantities from the interpolation function were calculated from these windowed sections. The same low relative density of S = 2.0 was used for these calculations. The *Sk* and *As* parameters were calculated from the Ursell number based approach discussed in section 3.2, thus the input to the mobility and burial model has the same mean currents, but spatially smoother *Sk* and *As* input (Figure 12). The results are remarkably similar to the phase resolved models with less variation in UXO location on the wave and wave group time scale since some of this variability is averaged out with the sliding window calculations. In particular, the convergence location is almost the same as the previous method, and a similar power law relation (b = 0.0134, m = 1.594, Figure 11) for final UXO location also fits this data well. This suggests that the interpolation function is a suitable method for transitioning from a wave resolved to wave-averaged approach.

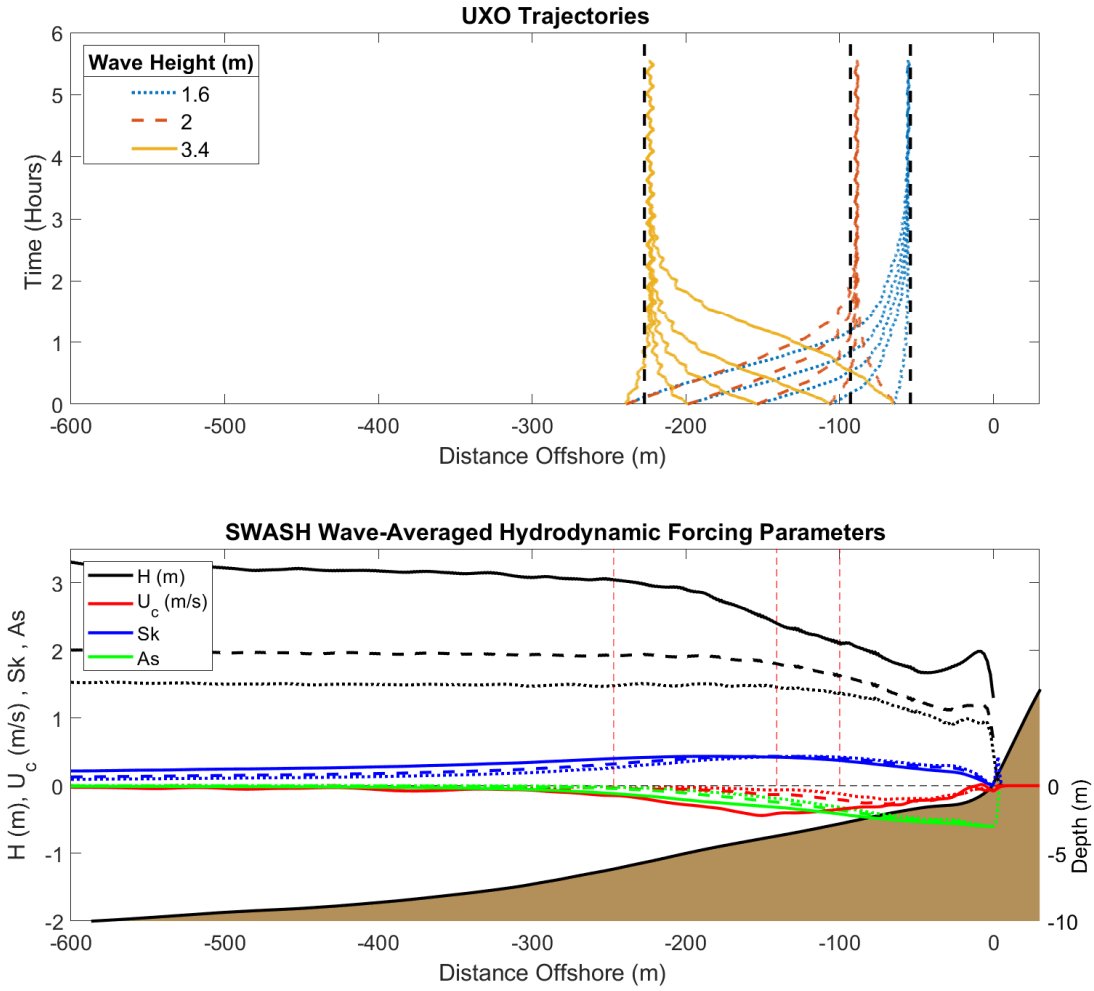

Figure 12. Results of SWASH wave-averaged UXO mobily and burial modelling. Upper Panel) Time series of UXO migration paths for the three different wave heights and five different intial conditions. A power law location (x_{bp}) related to the breaking index is shown as the vertical black dashed lines. Lower Panel) Hydrodynamic foring parameters including wave height (black), mean current (red) skewness (blue) and acceleration (green). The location (x_b) of the breaking point based on a breaker index is shown as the vertical red dashed lines.

4.2.2. XBeach Spectral Input

The UXO mobility model was run using the output of the Xbeach model for the same initial UXO density, locations and spectral wave heights as the SWASH runs. For these runs morphologic change calculations that are possible in Xbeach were disabled for a more direct comparison with SWASH. Since Xbeach produces wave-averaged output the sliding window calculation of wave-averaged variables is not required. The qualitative results are similar to the SWASH results with object initiating near the beach migration offshore with the large wave case and object initiating offshore migration onshore with the small wave case. The quantitative final

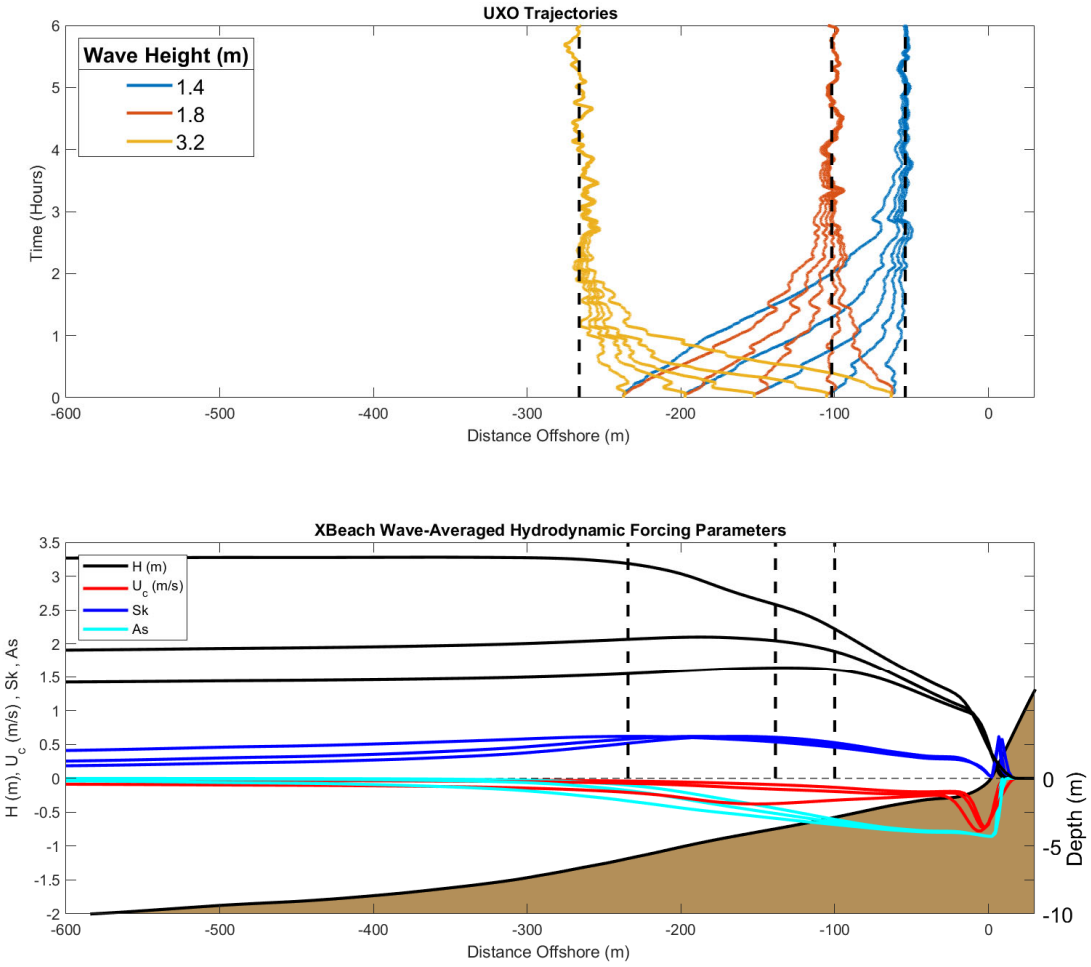

Figure 13. Results of Xbeach wave-averaged UXO mobily and burial modelling. Upper Panel) Time series of UXO migration paths for the three different wave heights and five different intial conditions. Lower Panel) Hydrodynamic foring parameters including wave height (black), mean current (red) skewness (blue) and acceleration (cyan).

locations of the UXO and power law coefficients (b = 0.0112, m = 1.846) are slightly different than those predicted by SWASH (Figure 11).

4.3. Xbeach and SWASH hydrodynamics

To further investigate the difference between the final UXO location in the SWASH wave-averaged and Xbeach results, the hydrodynamic output results were examined for the largest wave height input. Both wave-averaged modelling approaches used the same parametrized predictions of *Sk* and *As* based on Ursell number, which is a function of wave height, period, and water depth, thus the mean currents and wave heights were compared. The modelled wave heights are similar with the most significant difference in the swash zone since the Xbeach output does not include infragravity band energy while the Swash output has all bands. The mean currents are significantly different as the SWASH offshore directed currents reduce to smaller values (0.04 m/s for the bottom grid cell SWASH vs 0.1 m/s for Xbeach) outside the surf-zone.

Some of the differences are due to the depth resolution of the SWASH model. The depth averaged output of SWASH converges to a value of 0.06 m/s. This increased offshore velocity from the Xbeach model leads to a slightly further seaward final location (260 m) of the UXO under large wave forcing compared to the SWASH model (200 m).

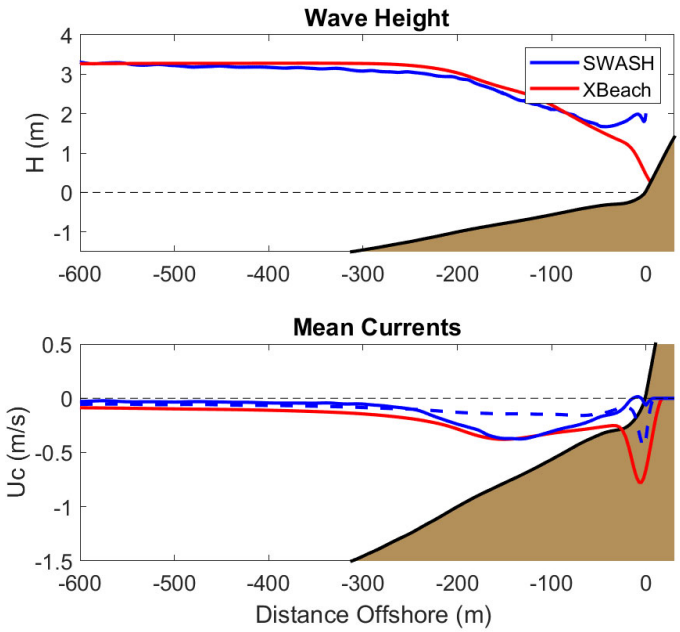

Figure 14. SWASH (blue) and Xbeach (red) hydrodynamics. Upper panel) Wave Height, Lower Panel) Mean currents. Dashed blue line is depth avegaged SWASH output, solid line in the bottom grid cell and solid blue line is the bottom grid cell

4.4. Realistic time series from field measurements

Both SWASH with the wave-averaged UXO mobility post-processing module and Xbeach were run with input from field observations taken during the 2014 and 2018 experiments on Martha's Vineyard. The initial locations ranged from x= -65 m offshore of the beach to -240 offshore of the beach corresponding to depth of 2 to 6 m. The center location of x = -150, D = 4 is similar to the center of the field deployment locations.

4.4.1. SWASH

The 2014 medium wave height (2.5 m at the peak of the storm, Left panels of Figure 15) SWASH results show onshore UXO migration at the beginning of the time series for all initial locations. As the waves and return flow currents increase in the onshore part of the domain after 1.5 hours, some of the UXO reverse direction and begin to migrate back offshore. Similar to the simulations with spectral forcing, all UXO converge to a common trajectory after 3 hours and remain mobile due to the low relative density (S = 2.0) of the UXO and consistently energetic forcing at the convergence location. The convergence location is at the break point where onshore forcing due to wave skewness and acceleration balances offshore directed mean flows. The largest field measured onshore migration was 120 m for this event consistent with the predicted migration of the objects initialized offshore of x = -120 m before the reversal. SWASH does not have any morphology changes so any onshore sand bar migration that may have buried the objects at their maximum landward location is not included in the SWASH predictions.

In the SWASH hindcasts of the 2018 data set with H = 3.5 m waves at the peak of the storm, the UXO initiated at 4 m (x_i = -170 m Figure 15, right, red line in the trajectory plot) and deeper had net migration offshore, the migration of the UXO initiated near 4 m depth show relatively little (20 m) offshore migration in the first 10 hours of the wave event, consistent with the 2018 measurements in which little migration was measured. At 14 hours all the UXO converged on a common trajectory. At 20 hours into the simulation, at the peak of wave height, all UXO rapidly migrated offshore, which was not observed in the field measurements. These SWASH simulations do not have morphodynamics, and thus do not predict the observed offshore migration of a sandbar which buried even the low relative density (S =2.0) UXO up to 1.5 m deep. Based on light sensors on the field deployed UXO, the sand bar migration induced burial occurred before 15 hours, thus this burial could explain the difference between the SWASH simulations with no morphodynamics and the measurements. The simulations did not predict burial in this case with low relative density (S =2.0) UXO. In the next section simulations with Xbeach, that does have the ability to predict sand bar migration, will be discussed. XBeach is also much less computationally expensive than SWASH so allows longer duration simulations over a wider range of input parameters.

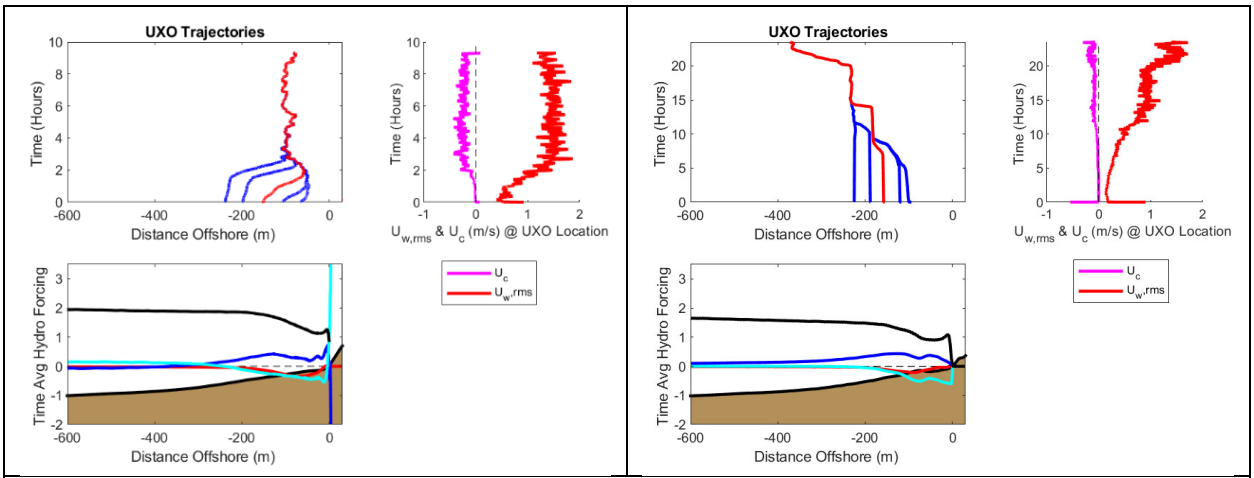

Figure 15. SWASH 2014 (left) and 2018 (Right) Field Time Series UXO mobility hindcasts. The upper left plots are UXO cross shore location as a function of time. The upper right plots are r.m.s. wave (red line) and current (magenta) at the location of the UXO. Lower left plots show the cross-shore dependence of forcing parameters with the same colors as Figure 13 at the peak of the storm

4.4.2. XBeach

XBeach simulations with forcing from the 2014 field experiment conditions show morphodynamic change in the near shore part of the domain (Figure 16). From t = 5 hours to 30 hours sand is eroded from the region between x = -100 and x -30 and deposited onshore of x = -30. The erosional zone would tend to inhibit burial, and while the depositional zone would tend to enhance potential for burial. In this case, the depositional zone is associated with steep slopes thus potentially enhancing gravitational forcing of UXO rolling offshore.

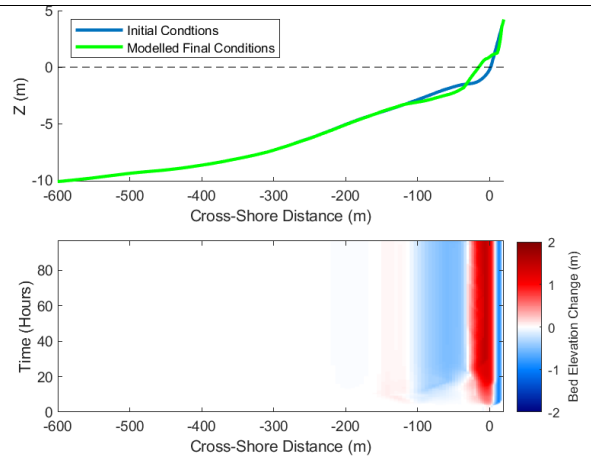

Figure 16. Morphodynamic change predicted by Xbeach for the 2014 field measurement forcing conditions

The UXO mobility post-processing module was run with a variety of initial conditions and input parameters. Similar to the SWASH runs with initial UXO locations were spaced from $D = 2$ m to 6 m in 1 m steps. Three different values of the parameter α, which scales the burial time constant, were used with values of 0.1 .25 and 0.5 in each column of Figure 17. In the mobility and burial post processing of the Xbeach data shown in Figure 17 morphodynamic change was not included. Eight different relative densities were used ranging from $S = 1.5$ to 4 in with steps of 0.36, which are shown in the rows of Figure 17. For the $\alpha = 0.1$ case, only the least dense UXO ($S = 1.5$ and 1.9) were mobile and the denser UXO buried quickly. The burial decreased slightly after 30 hours, but not enough for the UXO with S greater than 1.9 to become mobile. For the $\alpha = 0.25$ case, additional mobility of UXO with $S = 2.2$ and 2.6 is predicted. Some of the UXO in this density range with initial location further offshore migrate onshore, while the objects initiated further onshore bury without becoming mobile. This is due to the more rapid increase of wave velocity at the seafloor at the offshore sites. Once these UXO migrate onshore they bury to 50% burial depth and are no longer mobile. The $\alpha = 0.25$ results are consistent with the measurements that show onshore migration of UXO in this relative density range. For the $\alpha = 0.50$ case, additional onshore migration of objects with density less than $S = 3.3$ is predicted. This is inconsistent with measurements in which object above $S = 2.5$ rarely migrated, suggesting the tuning parameter α should be set to value near 0.25.

The mobility and burial post processing model was run on the same Xbeach with morphology included in the post processing. To contrast the difference between simulations without and with morphological change activated the two simulations for $\alpha = 0.25$ are shown in Figure 18. The most noticeable difference is the UXO which migrated into the nearshore region just outside the swash becomes more deeply buried (150% of its diameter) with morphologic change on due the nearshore accretion compared to the simulation with no morphologic change, in which burial is capped at 50%.

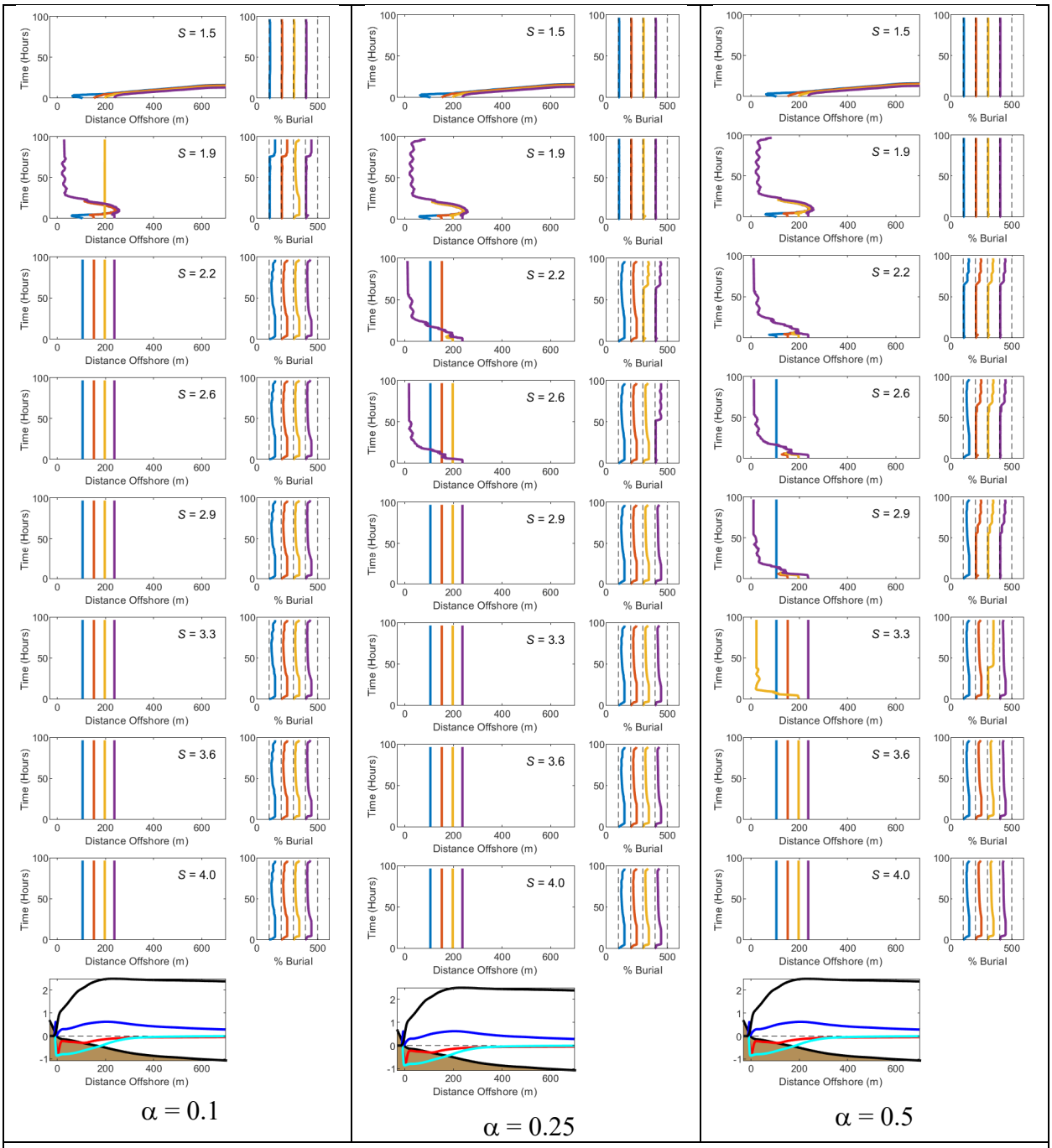

Figure 17. Xbeach Wave-averaged UXO mobility post processing results with the 2014 field measurement forcing conditions. The three columns represent different values of the parameter α and the rows show increasing relative density simulations. For each simulation, the trajectory (x-location vs time) is shown on the left as well as the time history of burial state on the right.

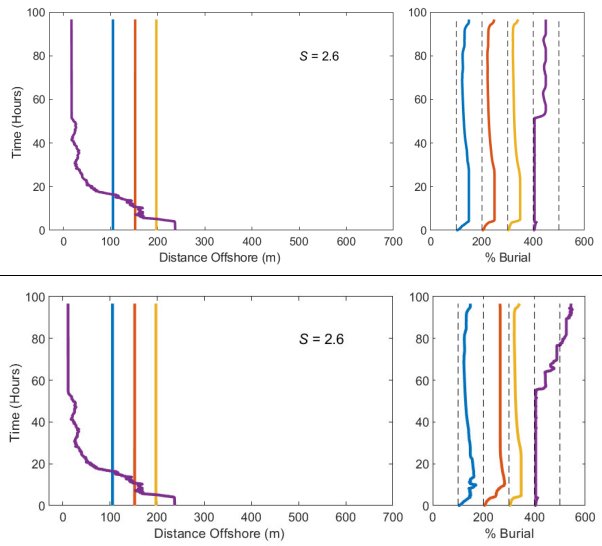

Figure 18. Comparison of Xbeach Wave-averaged UXO mobility post processing results with $\alpha = 0.25$ for $S = 2.6$ with morphology off (upper panel) and activated (lower panel) the morphological change of the seabed causes deep burial.

XBeach simulations with forcing from the 2018 field experiment conditions show more significant morphological change due to the large waves ($H = 3.5$ m), which forced offshore sand bar migration (Figure 19). The model slightly over-predicts the extent of the offshore bar migration and creates a lower amplitude wider bar than observed in the measurements.

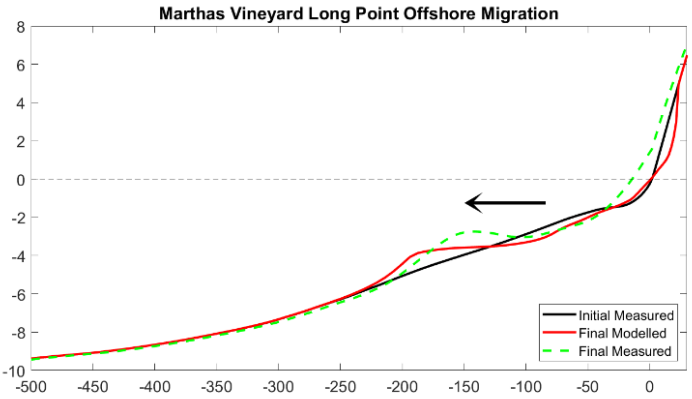

Figure 19. Morphodynamic change predicted by Xbeach for the 2018 field measurement forcing conditions

The initial locations of the UXO, the range of densities and range of values for the parameter α are the same as in the 2014 simulations. The results shown in (Figure 20) include the effects of changing bed morphology and are quite different from the 2014 results due to the more energetic wave forcing and offshore sand bar migration. All the low density ($S <= 1.9$) are highly

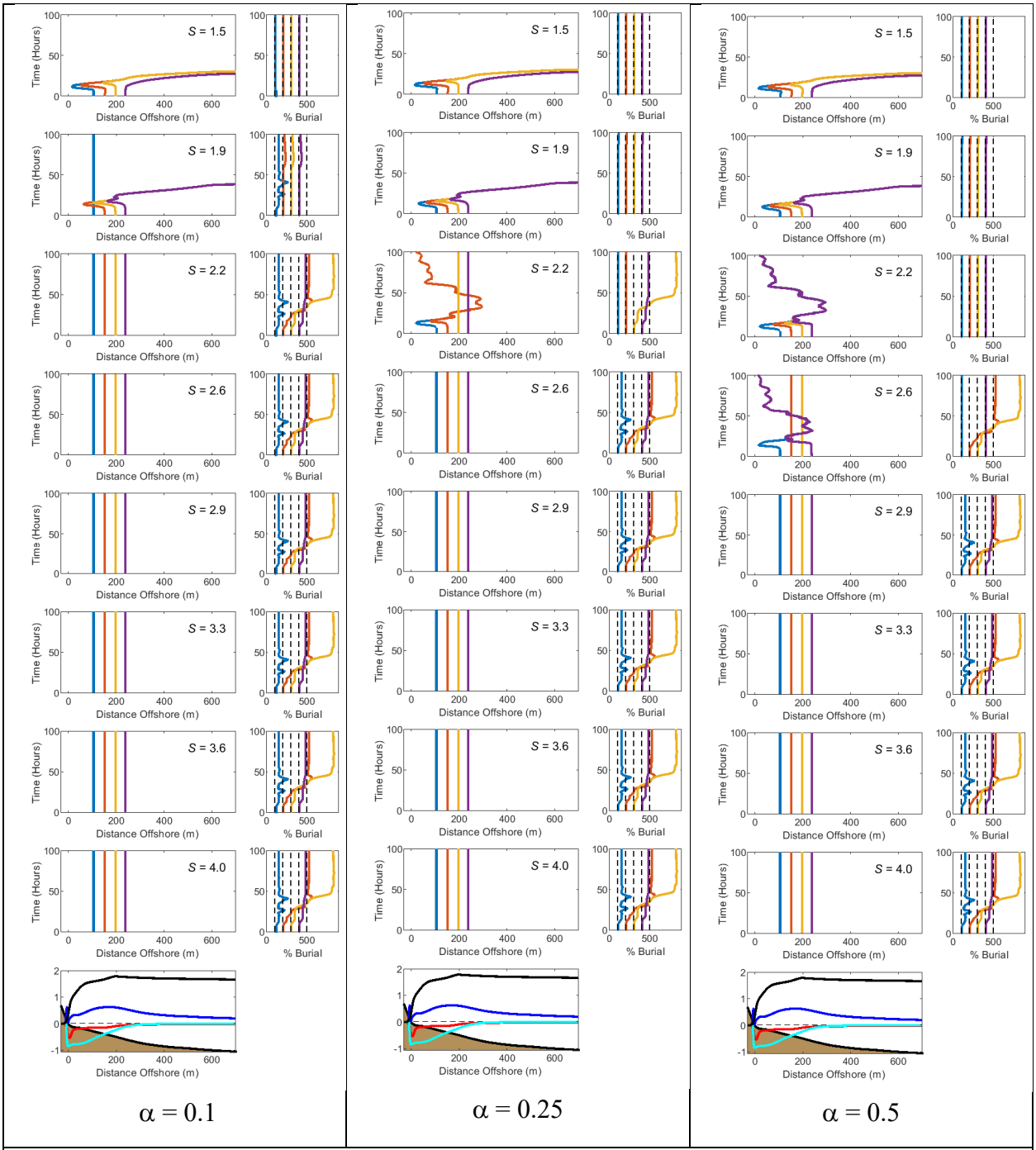

Figure 20. Xbeach Wave-averaged UXO mobility post processing results with the 2018 field measurement forcing conditions. The three columns represent different values of the parameter α and the rows show increasing relative density simulations. For each simulation, the trajectory (x-location vs time) is shown on the left as well as the time history of burial state on the right.

mobile and roll offshore at peak of the storm due the offshore directed mean currents. For the *S* = 2.2 density case, the behavior depends on the choice of the parameter α. For the α = 0.1 case

all UXO are stationary and the ones with initial location under the final sandbar location become deeply buried. For the $\alpha = 0.25$ case, the UXO initialized in the onshore part of the domain first migrate offshore and then return onshore as the offshore directed mean currents at the peak of the storm subside. For the $\alpha = 0.25$ case, the UXO initialized in the offshore part of the domain are buried by the migrating sand bar and are stationary. For the $\alpha = 0.5$ case UXO with densities up to 2.6 are mobile inconsistent with observations. For all values of α, UXO with densities of $S > 2.6$ are stationary and those under the sand bar become deeply buried. The simulations with $S = 2.6$ and $\alpha = 0.25$ best capture the differences in observed behavior between the 2014 and 2018 data sets, with no UXO migration in the 2018 simulations and onshore migration of some of the UXO in the 2014 simulations (Figure 21).

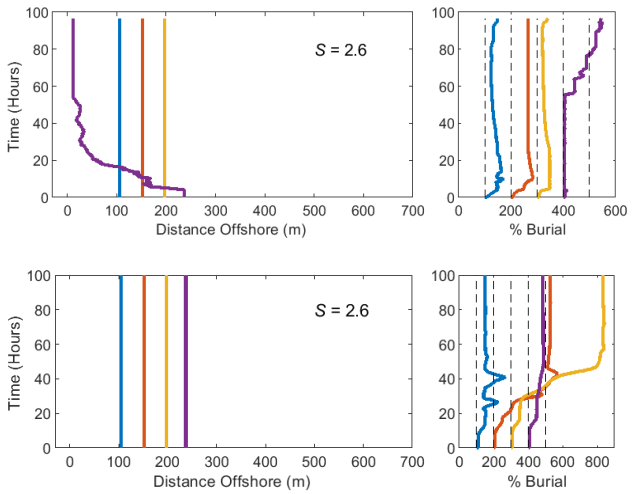

Figure 21. Comparison of Xbeach Wave-averaged UXO mobility post processing results with $\alpha = 0.25$ and $S = 2.6$ with morphology on for the 2014 measurements (upper panel) and 2018 measurements (lower panel). With the same parameters but different hydrodynamic forcing the model simulations show onshore mobility in 2014 followed by burial by sand bars and no mobility and deep burial due to migrating sand bars in 2018. The simulation results are consistent with measurements from both field deployments.

5. Conclusions and Implications for Future Research/Implementation

The approach of using a wave-averaged nearshore hydrodynamics model with a parametrized mobility and burial post-processing model module that is derived from wave resolved simulations appears to have ability to hindcast observed UXO mobility and burial behavior from two different sets of observations with the correct choice of tuning parameters. The wave-averaged nearshore hydrodynamics model (in this case Xbeach) is computationally efficient and provides predictions of morphodynamic change which is essential for burial predictions. While there are many parameters that could be tuned, the mobility and burial post-processing model is most sensitive to the parameter α, which scales the time constant on the non-equilibrium burial model. Selecting high values of this parameter results in burial that lags the predicted equilibrium scour and enhanced mobility. Low values result in similar prediction to the equilibrium burial model which typically predicts less mobility than observed. While the simulations with forcing based on measurements have complex time dependence due to time varying input, the simulations with constant wave height forcing generally suggest that low

density UXO migrate in a similar manner to sand bars. In moderate wave energy conditions sand bars tend to migrate onshore due to weak undertows and breaking near the beach and in more energetic conditions the sand bars migrate offshore due wave breaking further offshore and stronger returns flow. Additional observations planned for 2023 with initial locations in a cross-shore distributed array will evaluate this hypothesis.

Future work to extend the approach to simulations resolving along and across-shore processes is relatively straight forward conceptually and would be useful to test if models can predict the lack of along-shore UXO migration observed in these data sets and make predictions about expected along-shore migration in locations with stronger along shore currents.

Since the wave-averaged hydrodynamic modelling combined with parameterized mobility and burial modelling approach is relatively computationally efficient it could provide a basis for monte-carlo simulations spanning a wide variety of input parameters for input into statistical models such as UnMES (Underwater Munitions Expert System [15])

References:

[1] P. Traykovski, "MR-2319: Continuous Monitoring of Mobility, Burial and Re-Exposure of Underwater Munitions in Energetic Near-Shore Environments." [Online]. Available: https://www.serdp-estcp.org/Program-Areas/Munitions-Response/Munitions-Underwater/MR-2319/MR-2319/(language)/eng-US. [Accessed: 04-Jan-2021].

[2] P. Traykovski and F. Jaffre, "Rapid Response Surveys of Mobility, Burial and Re-Exposure of Underwater Munitions in Energetic Surf-Zone Environments and Object Monitoring Technology Development MR-2729 Final Report," WOODS HOLE OCEANOGRAPHIC INSTITUTION MA, 2020.

[3] J. Calantoni, T. Staples, A. Sheremet, and U.S. Naval Research Laboratory, "Long time series measurements of munitions mobility in the wave-current boundary layer," U.S. Naval Research Laboratory, Mar. 2014.

[4] A. Shields, "Application of similarity principles and turbulence research to bed-load movement," 1936. [Online]. Available: https://authors.library.caltech.edu/25992/1/Sheilds.pdf. [Accessed: 15-Dec-2022].

[5] S. E. Rennie, A. Brandt, and C. T. Friedrichs, "Initiation of motion and scour burial of objects underwater," *Ocean Eng.*, vol. 131, pp. 282–294, Feb. 2017.

[6] C. Friedrichs, S. E. Rennie, and A. Brandt, "Self-burial of objects on sandy beds by wave- and current-induced scour," 2016.

[7] Y. A. Cataño-Lopera and M. H. García, "Geometry of scour hole around, and the influence of the angle of attack on the burial of finite cylinders under combined flows," *Ocean Eng.*, vol. 34, no. 5, pp. 856–869, Apr. 2007.

[8] P. Nielsen, *Coastal Bottom Boundary Layers and Sediment Transport*. World Scientific, 1992.

[9] R. Whitehouse, *Scour at Marine Structures: A Manual for Practical Applications*. Thomas Telford, 1998.

[10] P. Traykovski, "Observations of wave orbital scale ripples and a nonequilibrium time-dependent model," *J. Geophys. Res. C: Oceans*, vol. 112, no. C6, 2007.

[11] E. Meyer-Peter and R. Müller, "Formulas for bed-load transport," *IAHSR 2nd meeting, Stockholm*, 1948.

[12] T. Abreu, P. A. Silva, F. Sancho, and A. Temperville, "Analytical approximate wave form for asymmetric waves," *Coast. Eng.*, vol. 57, no. 7, pp. 656–667, Jul. 2010.

[13] B. G. Ruessink, G. Ramaekers, and L. C. van Rijn, "On the parameterization of the free-stream non-linear wave orbital motion in nearshore morphodynamic models," *Coast. Eng.*, vol. 65, pp. 56–63, Jul. 2012.

[14] Y. Goda, "Reanalysis of Regular and Random Breaking Wave Statistics," *Coast. Eng. J.*, vol. 52, no. 1, pp. 71–106, Mar. 2010.

[15] S. Rennie and Johns Hopkins Applied Physics Laboratory Baltimore United States, "Underwater munitions expert system to predict mobility and burial," Johns Hopkins Applied Physics Laboratory Baltimore United States, Nov. 2017.